JIMMA UNIVERSITY

COLLEGE OF NATURAL SCIENCES

DEPARTMENT OF CHEMISTRY

PHOTOCATALYTIC DEGRADATION OF METHYLENE BLUE DYE USING CUPROUS OXIDE/GRAPHENE NANOCOMPOSITE

BY: BEKAN BOGALE DUKI

NOVEMBER, 2021

JIMMA, ETHIOPIA

PHOTOCATALYTIC DEGRADATION OF METHYLENE BLUE DYE USING CUPROUS OXIDE/GRAPHENE NANOCOMPOSITE

A THESIS

SUBMITTED TO SCHOOL OF GRADUATE STUDIES, JIMMA UNIVERSITY IN PARTIAL FULFILMENT OF THE REQUIREMENTS FOR THE DEGREE OF MASTER OF SCIENCE IN CHEMISTRY (PHYSICAL CHEMISTRY)

BY: BEKAN BOGALE DUKI

ADVISORS: FEKADU MELAK (PhD)

TSEGAYE GIRMA (PhD)

TILAHUN YAI (MSc**)**

NOVEMBER, 2021

JIMMA, ETHIOPIA

Declaration

I hereby declare that, this thesis entitled "**PHOTOCATALYTIC DEGRADATION OF METHYLENE BLUE DYE USING CUPROUS OXIDE/GRAPHENE NANOCOMPOSITE**" and the work presented in it are my original work and has not been presented for a degree in any other university and that all sources have been appropriately acknowledged.

Student's Name: **Bekan Bogale Duki**

Signature: _____

Date: _____

Name of adviser: **Fekadu Melak (PhD)**

Signature: _____

Date: _____

November, 2021

Jimma, Ethiopia

Approval Sheet

The thesis entitled "**PHOTOCATALYTIC DEGRADATION OF METHYLENE BLUE DYE USING CUPROUS OXIDE/GRAPHENE NANOCOMPOSITE**" by Mr. Bekan Bogale Duki is approved for the degree of Master of Science in Chemistry.

APPROVED BY BOARD OF EXAMINERS

	Signature	**Date**
Advisers: **Fekadu Melak (PhD)**	_____	_____
External examiner: _____	_____	_____
Internal examiner: _____	_____	_____
Chairman: _____	_____	_____

November, 2021

Jimma, Ethiopia

TABLE OF CONTENTS

ACKNOWLEDGMENT

I would like to express my heartfelt gratitude to my research supervisors, Fekadu Melak (PhD), Tsegaye Girma (PhD), and Tilahun Yai (MSc) for their endless guidance, encouragement, motivation, patience, and continuous supports throughout my thesis journey. My heartiest gratitude also goes to my beloved family for all their love and continuous encouragement. I would also like to convey many thanks to my brother, Felmeta Bogale**,** I have no doubt that without your selfless love and endless support; it was not possible to achieve this goal. Finally, I would like to thank the Chemistry Department and staff members of the department, my classmates, and friends who shared their experiences, valuable information, and materials. My special gratitude goes to Jimma University for financial support during my study.

LIST OF FIGURES

LIST OF TABLES

ABBREVIATIONS AND ACRONYMS

FTIR	Fourier transformed infrared
NCs	Nanocomposites
NPs	Nanoparticles
PXRD	Powder X-ray Diffraction Analysis
SEM	Scanning electron microscopy
TEM	Transmission Electron Microscopy
RGO	Reduced Graphene oxide
GO	Graphene Oxide
eV	Electron Volt
MB	Methylene Blue
VB	Valance Band
CB	Conduction Band

ABSTRACT

The stability of Cu_2O nanoparticles due to the fast recombination rate of electron/hole pairs remains a significant challenge in its photocatalytic applications for water treatment. In this study, Cu_2O/graphene nanocomposite was prepared for photocatalytic degradation of methylene blue (MB) dye. Cu_2O/graphene nanocomposites were synthesized from graphite powder and copper nitrate using the facile sol-gel method. In addition, initial process parameters such as contact time, catalyst dosage, and pH of the solution were examined for MB removal. The prepared hybrid nanocomposites were characterized using UV-Vis, FT-IR, XRD, and SEM instruments. The photocatalytic activities of Cu_2O nanoparticles and Cu_2O/graphene nanocomposite were compared for cationic methylene blue (MB) dye degradation. Cu_2O/graphene nanocomposite exhibits higher photocatalytic activity on MB (with a removal efficiency of 94%) than bare Cu_2O nanoparticles (67%). The kinetic study of the MB degradation process confirmed that the second-order kinetic model fits the experimental data. Thus, this work indicated new insights into Cu_2O/graphene nanocomposite as high-performance in photocatalysis to degrade MB, playing a great role in environmental protection in relation to MB dye.

Keywords: *Methylene blue, Photocatalysis, Cuprous Oxide, Cuprous Oxide/Graphene Nanocomposite*

1. INTRODUCTION

Pollution has become unavoidable in the recent lifestyle due to a fast industrial and technological development. The wastewaters discharged from textile industries includes residual dyes (which are poorly biodegradable) cause water pollution and serious threat to the environment [1]. Methylene blue (MB) dye is a basic aniline dye, $C_{16}H_{18}N_3SCl$ that forms a deep blue solution when dissolved in water. MB is a biologically active substance, and if not treated before discharged to a water body, it can lead to several health complications, including gastrointestinal disturbances and dysuria [2,3]. Therefore, the efficient treatment of wastewaters has become of immediate importance among the scientific community around the globe as there is a growing need to come out with the state of the art technologies that are capable to solve the problems [4].

Nowadays, various methods such as photocatalysis [5], microbial degradation [6], hydrolytic degradation [7], chemical decontamination [8], and adsorption [9] have been developed for the treatment of these dyes. Among these methods, photocatalytic technology is one of the most effective methods for wastewater treatment because of its simple process and green technology, low investment cost, mild reaction conditions, and degrade dyes into non-hazardous products [10]. Although, photocatalytic applications which produce negligible secondary pollution have been intensively reported in many literatures [10,11,12]. Moreover, photocatalytic degradation methods have enticed immense attention owing to their capability to utilize UV–visible or solar light for the production of photo-generated electron-hole pairs. The produced electron-hole pairs form reactive oxygen species (ROS) which are highly reactive and capable of destroying organic and inorganic pollutants as well various microorganisms including bacteria, viruses, spores, and protozoa, etc [14].

Recently, semiconductor photocatalysis is one of the most promising processes for the treatment of contaminated water using MB [15]. Several semiconducting metal oxide materials including TiO_2 [16], ZnO [17], Fe_2O_3 [18], WO_3 [19], Cu_2O [20] have been investigated for their good photocatalytic organic waste treatment activities. Among those catalysts, cuprous oxide (Cu_2O) is a p-type semiconductor that is nontoxic, low cost, and has abundant source materials [21]. It has been demonstrated that Cu_2O has good application prospects in photocatalysis, solar energy cell, hydrogen production, and anode material for lithium-ion batteries [21,22,23]. However, excited electron-hole pairs are not with the

effective bandgap separation and this leads to the fast recombination rate which tends to reduce the photocatalytic activity. To overcome these problems, graphene has been widely explored as a supporting material improving the photo-catalyst performances [25].

Graphene, with a unique two-dimensional sp^2-hybridized single layer carbon structure, possesses many fundamentally interesting electronic properties such as zero bandgaps, zero effective mass, high charge carrier mobility, large surface area, and high optical transparency over a very large spectral range from IR to UV, which makes it an excellent candidate for enhancing the performance of photocatalysts and significantly improve the separation efficiency of photogenerated electron-hole (e^-/h^+) pairs in photocatalytic processes [25,26].

As a photocatalyst carrier, graphene forms an electrical conducting network so that the photogenerated electrons could easily be transferred and decrease the recombination of photogenerated e^-/h^+pairs. Moreover, graphene could prevent aggregating, leading to increasing the surface area of photocatalysts, thus improving the photocatalytic property of Cu_2O nanostructures significantly [28]. Besides its remarkable electronic properties, recombination of electron-hole pairs can be prevented in Cu_2O/graphene nanocomposite through the formation of heterojunction (Schottky barrier) at the interface of the conjugated π-orbitals of graphene and Cu_2O conduction band. Graphene can act as an electron acceptor and trap the excited electrons which reduce the recombination rate by separating electron-hole pairs [29]. Moreover, photocatalytic degradation attempts of MB via Cu_2O /graphene nanocomposite are seldom reported. In view of this observation, Cu_2O/graphene nanocomposite was synthesized, characterized, and its photocatalytic activity was evaluated by the photodegradation of MB dye under visible light.

1.2 Statement of the Problem

Rapidly increasing concentrations of organic pollutants such as synthetic dyes in different kinds of water sources have widely increased concerns worldwide [30]. Discharging of wastewater effluents that are contaminated with MB to water resources without efficient degradation results in harmful effects, such as burns of the eye, nausea, vomiting, and diarrhea [31]. Therefore, finding an effective treatment method for wastewater containing dye (MB) should be developed.

Semiconductor photocatalysts may play a great role in the photocatalytic degradation of organic pollutants (dyes) in wastewater. Metal oxide semiconductors are the most often studied materials in photocatalysis owing to their high photocatalytic activity, non-toxicity, and chemical stability [32]. Cu_2O nanoparticles are among the well-known metal oxide photocatalyst and most active photocatalysts for the degradation of a wide range of organic compounds. However, it has fast recombination of photogenerated electrons and holes, which limits its performance. To overcome these limitations, graphene may be a favorable additive for making nanocomposites with cuprous oxides, to inhibit the fast recombination of electron-holes pairs. Despite such exceedingly higher transformation induced by graphene, studies focused on photocatalytic activity of Cu_2O/graphene nanocomposite upon several organic dye molecules such as MB are seldom reported.

1.3 Objectives

1.3.1 General Objective

To synthesize, characterize, and evaluate photocatalytic activity of Cu_2O/graphene nanocomposite

1.3.2 Specific Objectives.

- To synthesize the Cu_2O/graphene nanocomposite using the facile sol-gel method
- To characterize the synthesized Cu_2O/graphene nanocomposite using UV-Vis, FTIR, XRD, and SEM spectroscopic techniques.
- To study the influence of reaction conditions (temperature, graphene amount, and reaction time) on structural, and optical properties of Cu_2O/graphen nanocomposite.

- To study photocatalysis influencing parameters on the photocatalytic degradation of MB
- To investigate the photocatalytic degradation efficiency of MB using Cu_2O/graphene nanocomposite

1.4 Significance of the Study

Nanotechnology innovation is the quickest developing division of technology with multiple consumer products. Its little size and extensive surface area per unit volume impart characteristics that can be useful in photocatalytic construction. Cuprous oxide nanoparticles (Cu_2ONPs) application is a very promising, efficient, and cost-effective method for remediating this environmental health concern. Therefore, there is a need to synthesize Cu_2O/graphene nanocomposite photocatalyst for the photodegradation of organic pollutants such as MB before being discharged to the environment.

Moreover, the findings of this research may be used for:

- Upgrading the knowledge about the Cu_2O/graphene nanocomposite regarding its photocatalytic activity.
- Setting the ground for further investigation of chemical and health aspects of Cu_2O/graphene nanocomposite.
- Providing further awareness for researchers about the kinetic degradation action of Cu_2O/graphene nanocomposite.

2. REVIEWS OF RELATED LITERATURE

2.1. Water Contamination and Demand for Solution

Water contamination is one of the most serious environmental issues, as many hazardous micropollutants such as heavy metals, pharmaceuticals, dyes, fertilizers, and pesticides are increasingly being released into the watercourses [33]. In the global scenario, the textile industry is considered one of the largest water polluters by releasing a huge number of dyes into the water system. The biggest challenge in this issue is that these dyes are highly stable and remain unaffected even after chemically and biologically treated [1]. Therefore, several advanced techniques have been used to deal with this serious phenomenon, such as biological, wet catalytic oxidation, ozonation, electrochemical, son catalytic, photochemical techniques, etc.,[17,18] were used to remove organics from wastewaters, but still have the challenge to complete elimination of this refractory organics [36].

Photocatalysis utilizes renewable, clean, and inexhaustible radiations of the sun for the activation of chemical reactions by oxidation and reduction, hence it becomes a versatile, easy to use, and economical technology in the wastewater treatment processes [37]. Heterogeneous photocatalysis, a category of advanced oxidation processes (AOPs), works well with the help of inorganic photocatalyst (semiconductors) and light energy. Upon illumination by light, electron-hole pair is generated respectively in conduction and valence bands of the photocatalyst. These photo-generated charge carriers react with surface molecules (such as H_2O, adsorbed O_2) to undergo secondary reactions to produce the radical species ($^{\cdot}OH$, O^{2-}) which further react with the organic compounds and reduce them to harmless products such as H_2O and CO_2 [30].

Cuprous oxide (Cu_2O) is a p-type semiconductor with an arrow bandgap of 2.1eV which has been widely used in various fields based on their unique magnetic, electronic, and optical properties, such as CO oxidation, gas sensing, photodegradation, photocatalyst, and so on [38]. With its advantages of low cost, abundant, non-poisonous and easy synthesis, Cu_2O has been widely researched as photocatalysis. However, the stability of Cu_2O is a serious issue as the redox potentials for the reduction and oxidation of monovalent copper oxide lie within the bandgap and the fast recombination rate of the photogenerated electron-hole pairs also hinders the industrial application of this semiconductor [39].

To overcome them, graphene material is one of the potential supports due to the large specific surface area[40]and high mobility of charge carriers [41]. Graphene can accept electrons to prevent recombination and provide a favorable surface area for absorption of dye through π-π conjugation between dye and aromatic region of graphene. The trapped electrons on graphene react with the dissolved oxygen and water to form reactive oxygen and hydroxyl radicals which further oxidize the dye [42].

2.2. Nanomaterials, Nanoscience and Nanotechnology

Nanoparticles (NPs) are materials with at least a dimension under 100 nm, a broad variety of matter materials included [43]. The unit of nanometre derives its prefix nano from a Greek word meaning "dwarf" or "extremely small." One nanometre span 3–5 atoms lined up in a row. Nanoparticles are not essentially a molecular element in themselves, but are composed of three layers: the core, the shell layer, and the surface layer, the core the central part of the NP, and the shell layer the core part and the environment surface [44]. Due to the outstanding features of the NPs these products were a cause of concern for scientists in multidisciplinary areas. Nanoscale materials often present properties different from their bulk counterparts, as their high surface-to-volume ratio results in an exponential increase of the reactivity at the molecular level. Such properties include electronic, optical, and chemical properties, while the mechanical characteristics of the nanoparticles (NPs) may also differ extensively [45]. This enables them to be an object of intensive studies due to their academic interest and the prospective technological applications in various fields [46].

Nanostructure science and technology is accepted as a broad area of research and development activity that has been growing explosively worldwide in the past few years [47]. Nanotechnology is the science of the small; the very small. It is the use and manipulation of matter on a tiny scale. At this size, atoms and molecules work differently and provide a variety of surprising and interesting uses. It is an emerging interdisciplinary area that is expected to have wide-ranging implications in all fields of science and technology such as material science, mechanics, electronics, optics, medicine, plastics, energy, aerospace, etc [48].

Nanotechnology should not be viewed as a single technique that only affects specific areas. Although often referred to as the 'tiny science', nanotechnology does not simply mean very small structures and products. Nanoscale features are often incorporated into bulk materials

and large surfaces. Nanotechnology represents the design, production, and application of materials at atomic, molecular, and macromolecular scales, to produce new nanosized materials [49]. Such nanostructures may be synthesized by a wide number of methods, which involve mechanical, chemical, and other pathways.

2.3. Chemistry of Graphene and its Derivatives

Carbon-based materials are taking place in different fields ranging from composites to electronic devices. In recent years, the most preferred carbonic materials are graphene and carbon nanotubes (CNTs). These carbon allotropes show favorable results which can be seen as a very good alternative to other materials with their outstanding features such as easy functioning of the surfaces to provide various properties, high mechanical strength, and its unusual electronic properties, especially its possible technological applications [50].

2.3.1. Graphene

In recent years graphene, a one-atom-thick planar sheet of sp^2-bonded carbon atoms densely packed in a honeycomb crystal lattice, has grabbed appreciable attention to be used as a next-generation electronic material, due to its exceptional properties including high current density, ballistic transport, chemical inertness, high thermal conductivity, optical transmittance and super hydrophobicity at nanometer scale [51]. As compared to other carbon materials, graphene contain higher mobility (200000cm^2 v^{-1} s), young modulus (1TPa), and thermal conductivity ($4.84x10^3$ to $5.30x10^3$ W/mK) which make it a potential material in sector transistor element and integrated circuit, storage energy, gas sensor and bio electronic sensor [52]. Its robust electrical properties along with high optical transparency and flexibility make graphene a potential candidate in the applications such as touch-screens, liquid crystal display (LCD), photovoltaic cells, or organic light-emitting diodes (OLED) [53]. Graphene has potential in nano-applications in many scientific and industrial fields including the study of nano-electronics, molecular separation, composite additives, catalysis, nano-sensors, and transport [54].

2.3.2. Graphene Oxide

Graphene oxide (GO) has revealed some unique physicochemical properties such as small size, large surface area, exceptional strength in 2D structure, interesting optical and electronic properties, among others [55]. The structure of graphene oxide is similar to that of graphene, carrying a large number of active oxygen-containing functional groups, such as hydroxyl,

carboxyl, epoxy, etc., which enables GO to not only have the characteristics of graphene but also have other chemical and physical properties (for example, graphene oxide can be evenly and stably dispersed in water). At the same time, due to the introduction of oxygen-containing functional groups, the large π conjugate structure of graphene is destroyed, so the ability to conduct electrons is lost, and the conductivity is obviously reduced [56].

2.3.3. Reduced Graphene Oxide

Graphene oxide containing different oxygen groups could be reduced and result in a product called reduced-graphene oxide (rGO). This process could be performed using different approaches, including chemical reduction, microwave-assisted reduction, photo-reduction, thermal reduction, and solvothermal reduction [57]. Reduced-graphene oxide has few reduced sites as compared to the GO. Since rGO is prepared from the reduction of GO and there always remain some defects along with some oxygen functional groups within the structure or on the rGO surface. Both GO and rGO have excellent comparable properties, while rGO shows tuneable optical properties due to its functionality variability [58].

2.4. Graphene/ Metal Oxide Photocatalyst

Recently, a large number of studies have been published on the application of graphene/metal oxide nanocomposites as photocatalysts and for water, purification owing to its exceptional properties exhibited by the composites such as higher adsorptive, conductivity, tuneable optical behavior, stability, and longevity. Graphene and its derivative has been combined with a variety of metal oxides such as TiO_2, ZnO, and Cu_2O found to be an excellent photocatalyst for the degradation of synthetic dyes [59]

2.4.1 Graphene/Cu_2O Composite as Photocatalyst

Cuprous oxide (Cu_2O), which is a p-type semiconductor with a direct bandgap of 2.17 eV, has been widely studied as an efficient photocatalyst because of its abundance, low cost, environmental-friendliness and good visible-light response [60]. However, the stability of Cu_2O is a serious issue as the redox potentials for the reduction and oxidation of monovalent copper oxide lie within the bandgap [61] and the fast recombination rate of the photogenerated electron-hole pairs also hinders the industrial application of this semiconductor [62]. Due to this limitation, materials and methods for enhancing the photocatalytic efficiency of these semiconductors received great emphasis in photocatalysis research. Recent research revealed that conventional photocatalysts coupled with activated

carbon, fullerene, graphene, and other carbon-based material can largely improve the photocatalytic performance, among which the coupling with graphene showed noticeable and innovative results [63]

Sun et al.[64] Evaluated the addition of GO in the semiconductor with low loading of GO (0–0.5%) to enhance their photocatalytic activity under visible light irradiation. The photocatalytic activity of rGO/Cu_2O was reported exceeding that of pure Cu_2O. However, a further increase of graphene oxide content resulted in a gradual decrease in the photocatalytic activity due to the prevention of light from reaching the surface of the Cu_2O by the excessive GO, which would also shield the Cu_2O from absorbing visible light. Besides that, the loading of GO would inhibit the crystallization of Cu_2O that resulted in low photocatalytic activity.

A study by Benxia Li et al.[65] Showed that by combining reduced graphene oxide with Cu_2O, the light absorption range can be significantly extended to the visible light range and the electron-hole recombination rate can be suppressed as well. In the methylene blue (MB) photodegradation experiment, the rGO-Cu_2O photocatalyst showed much higher photocatalytic performance than bare Cu_2O. Effective charge transfers from the surface of Cu_2O to graphene that inhibited the recombination and therefore significant-high photocatalytic efficiency can be observed.

2.5. Methods of Graphene and its Derivatives Synthesis

The methods of producing high-quality graphene can be broadly categorized into two major classes, such as the “top-down” approach as well as “bottom-up” approach. The top-down approach is the most common method of producing large quantities of graphene at a low cost. It is synthesized by exfoliating natural or synthetic graphite using a strong oxidizing agent and followed by thermal exfoliation or chemical reduction [66]. The bottom-up approach consists of standard techniques such as epitaxial growth using metallic substrates using chemical vapour deposition (CVD) or organic synthesis which depend on the choice of precursor chemicals and thermal degradation and decomposition of the materials. Several other processes, such as arc discharge, chemical conversion CO reduction, CNT unzipping, and self-organization of surfactants have also been tried for the synthesis of graphene and its derivatives [67].

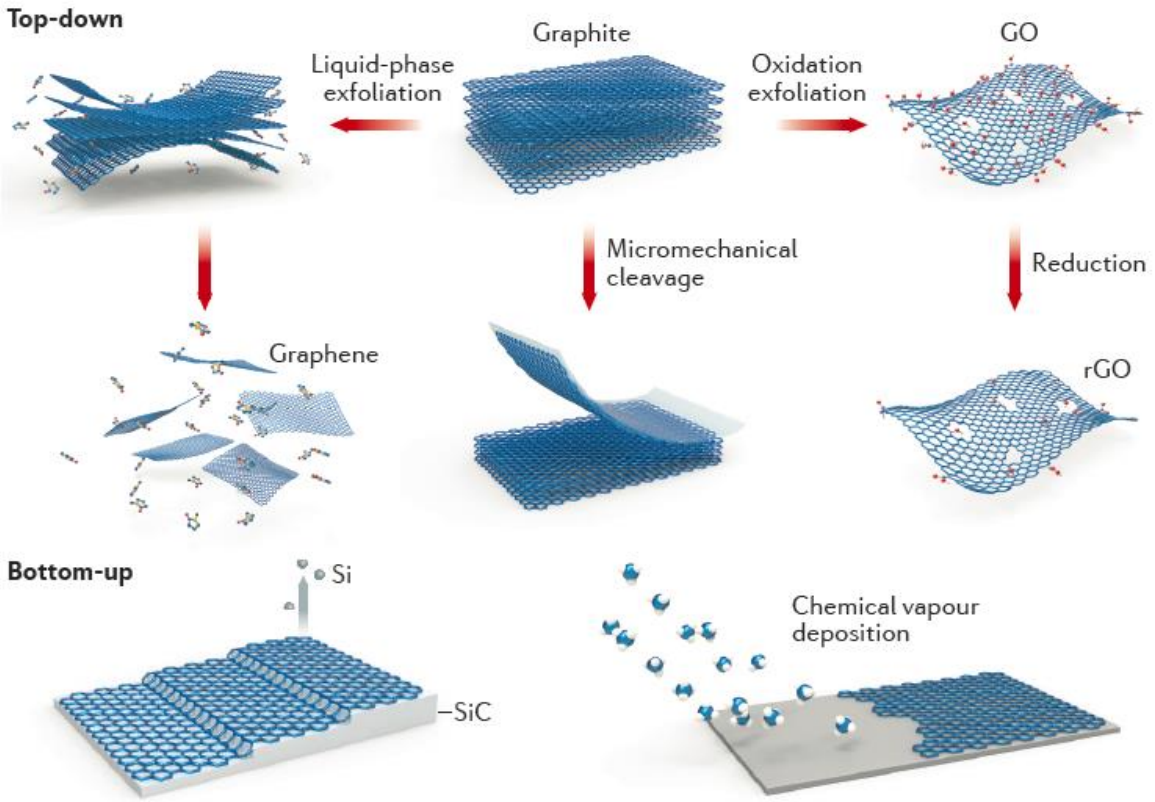

Figure 1: Top-down and bottom-up synthesis of graphene structures [68].

2.5.1 Synthesis of Graphene-Cuprous Oxide Nanocomposites

Cuprous oxide nanomaterial's have been synthesized by different techniques such as electrochemical, sonochemical combustion method, hydrothermal method, thermal decomposition, and microwave irradiation depending on the desired structure [69]. Mohd Shah et al.[70] Prepared Cu_2O/graphene nanocomposites in water using GO as a precursor for graphene and copper foil substrates as a single source precursor of Cu_2O under sol-gel condition. The whole process is simple, scalable, and industrially compatible.

2.6. Characterizations Graphene/Metal Oxide Nanoparticles

The great advances made in nanosciences and nanotechnology would not have occurred without the ability to characterize the nanoscale structural, chemical, and physical properties of materials. Moreover, the direct observation of nanostructure allows meaningful relationships between processing and properties to be made [71].

2.6.1. Ultraviolet-Visible (UV–Vis) Spectroscopy

UV-Vis spectroscopy (UV-Vis) is another relatively facile and low-cost characterization method that is often used for the study of nanoparticles in aqueous solution and solids by

analyzing the unique optical properties and optical bandgap which depends on the size and the shape of the nanoparticles between 200 nm to 800 nm. It measures the intensity of light reflected from a sample and compares it to the intensity of light reflected from a reference material [72].

2.6.2. Fourier Transformed Infrared (FTIR) Spectroscopy

FTIR spectroscopy is used to identify the possible functional groups of the active components present in the extracts or on the surface of NPs that are responsible for reducing, capping, and stabilizing being synthesized nanoparticles. The possible functional groups are identified in the ranges of 4000-400 cm^{-1}. The FTIR peaks attributed to stretching and bending vibrations are identified and assigned to determine the different functional groups present in the synthesized composite and the spectrum obtained is compared with a standard reference chart to identify functional groups present in the sample [42-46].

2.6.3. Energy Dispersive X-Ray Spectroscopy

Electron dispersive X-ray spectroscopy (EDS) was used for the determination of elemental composition and purity of the sample by atom %. Characteristic X-rays are emitted when the electron beam removes an inner shell electron from the sample, causing it to fill the shell and release energy [73]. These characteristic X-rays are used to identify the composition and measure the abundance of elements in the sample, the technique may know as EDX spectroscopy[74].

2.6.4. Powder X-ray Diffraction (XRD) Analysis

In a variety of X-ray spectroscopic modalities, XRD is a primary tool for completely resolving the tertiary structures of crystalline materials at the atomic scale. The diffraction of X-ray can be simply described as the reflection of a collimated beam of X-rays incident on the crystalline planes of an examined specimen according to Bragg's law [75]. XRD patterns were calculated using X per Rota flex diffraction meter using Cu K radiation and =1.5406 Å. Crystallite size is calculated using Scherrer equation:-

$$D = \frac{0.9\lambda}{B \cos \theta}$$

Where *D* is the particle size, λ is the X-ray wavelength, B is the full width of the half maxima (in radians) of the X-ray peak, and θ is the Bragg angle. Although XRD is routinely carried

out with standard laboratory diffractometers, it may be necessary to use synchrotron X-rays to obtain better resolution and sensitivity for materials such as metal oxides [76].

2.6.5. Scanning Electron Microscopy (SEM) Techniques

Scanning electron microscopy (SEM) was extremely useful for the determination of topology and observations of surfaces as they offer better resolution and depth of field than an optical microscope. SEM is a type of electron microscope that images the sample surface by scanning it with a high-energy beam of electrons in a raster scan pattern. The electrons interact with the atoms that make up the sample producing signals that contain information about the sample's surface topography, composition, and other properties such as electrical conductivity. The types of signals produced by an SEM include secondary electrons (SE), back-scattered electrons (BSE), characteristic X-rays, light (cathodoluminescence), specimen current, and transmitted electrons [77].

2.6.6. Transmission Electron Microscopy (TEM) Techniques

A transmission electron microscope is a complex setup in which a high-energy electron beam passes through a very thin specimen to be subsequently analysed. The transmitted portion of the electron beam is focused and magnified using electromagnetic lenses to form either a diffraction pattern or an image. It’s capable of imaging at a significantly higher resolution than light microscopes, owing to the small de Broglie wavelength of electrons. This enables the instrument's user to examine fine detail even as small as a single column of atoms, which is tens of thousands times smaller than the smallest resolvable object in a light microscope [44-47].

2.7. Dyes

Dyes have long been used in dyeing, paper and pulp, textiles, plastics, leather, cosmetics, and food industries. Color stuff discharged from these industries possesses certain hazards and environmental problems. These colored compounds for example (methylene blue, methylene orange, Congo red, etc.) are not only aesthetically displeasing but also inhibiting sunlight penetration into the stream and affecting the aquatic ecosystem, hence they have complex aromatic molecular structures which make them more stable and difficult to biodegrade[78]. Methylene Blue is a heterocyclic aromatic compound with molecular formula $C_{16}H_{18}ClN_3S$ as shown below, with IUPAC name 3,7 bis(Dimethylamino)-phenothiazin-5-ium chloride. MB is a cationic thiazine dye that is deep blue in the oxidized state while it is colorless in its

reduced form leucomethylene blue [2]. Methylene blue is a biologically active substance, and if administered inappropriately, it can lead to several health complications, including gastrointestinal disturbances and dysuria[79]. Therefore, various physical, chemical, and biological methods such as filtration, precipitation, coagulation, oxidation, and adsorption have been used to remove dyes[80]. In this study, cuprous Oxide- graphene (Cu_2O/graphene) nanocomposite have been used as a low-cost, efficient catalyst for the removal of MB dye from synthetic wastewater.

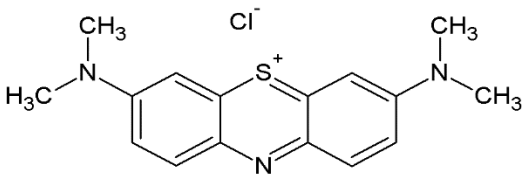

2.8. Photocatalysts

Photocatalysts are materials that, when absorbing photon energy, accelerate the rate of a reaction. It is, by the definition of a catalyst, neither consumed nor chemically changed in the reaction[81]. Over the past decades, photoactive nanomaterials as photocatalysts, especially semiconductor nanomaterials, have been of great interest due to their potential applications in environmental remediation and energy conversion [82]. Photocatalyst allows both spontaneous and non-spontaneous reactions, which relied on the photo-absorption ability of the material that can provide an energy source and turn it into chemical energy. As illustrated in Fig 2, the activity of photocatalyst (i.e., semiconductor) depends on the ability to create e^- and h^+ pairs to generate free radicals, which are needed to initiate the reaction. An electron from the valence band (VB) will be excited to the conductive band (CB) by absorption of the light energy equally or more than its bandgap, which is an energy difference between VB and CB in the semiconductor[83].

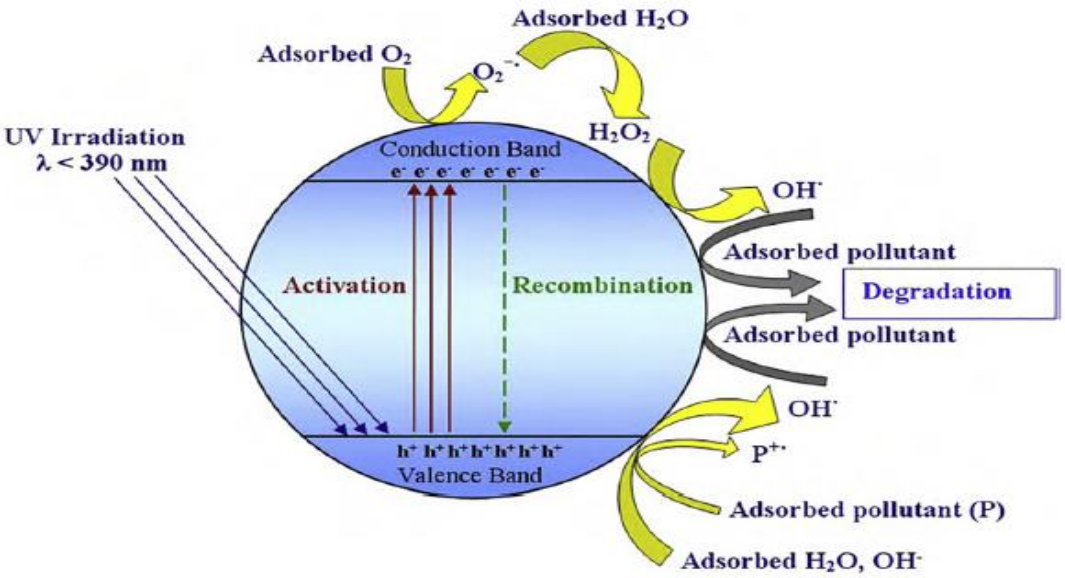

Figure 2. Simplification of photocatalysis mechanism

The photogenerated electron-hole pairs separate from each other and vigorously migrate to catalytically active sites at semiconductor surfaces where they reduce the electron acceptors or oxidize the donor species [84].

2.9. Mechanism of Photo-catalytic Degradation of Dyes

Dyes are the natural or artificial substances used for imparting or altering the color of a substance. Textile, printing, paper, rubber, paint, plastic, cosmetics, pharmaceutical, leather, and food industries use various dyes, and a portion of these dyes is discharged in wastewater that results in contamination of streams and waterways. Dyes are thus one of the important pollutants in the environment [85]. In environment cleaning applications utilizing photocatalytic forms, different sorts of semiconductor heterojunctions with distinctive morphologies play a vital role in the degradation of dyes or decolorization. The degradation of dyes depends on the charge separation and electron-hole combination. It has been stated that radical species generated during photoexcitation of the semiconductor are responsible for the degradation of dyes. The essential steps involved can be visualized (in a general sense) in the following steps [86].

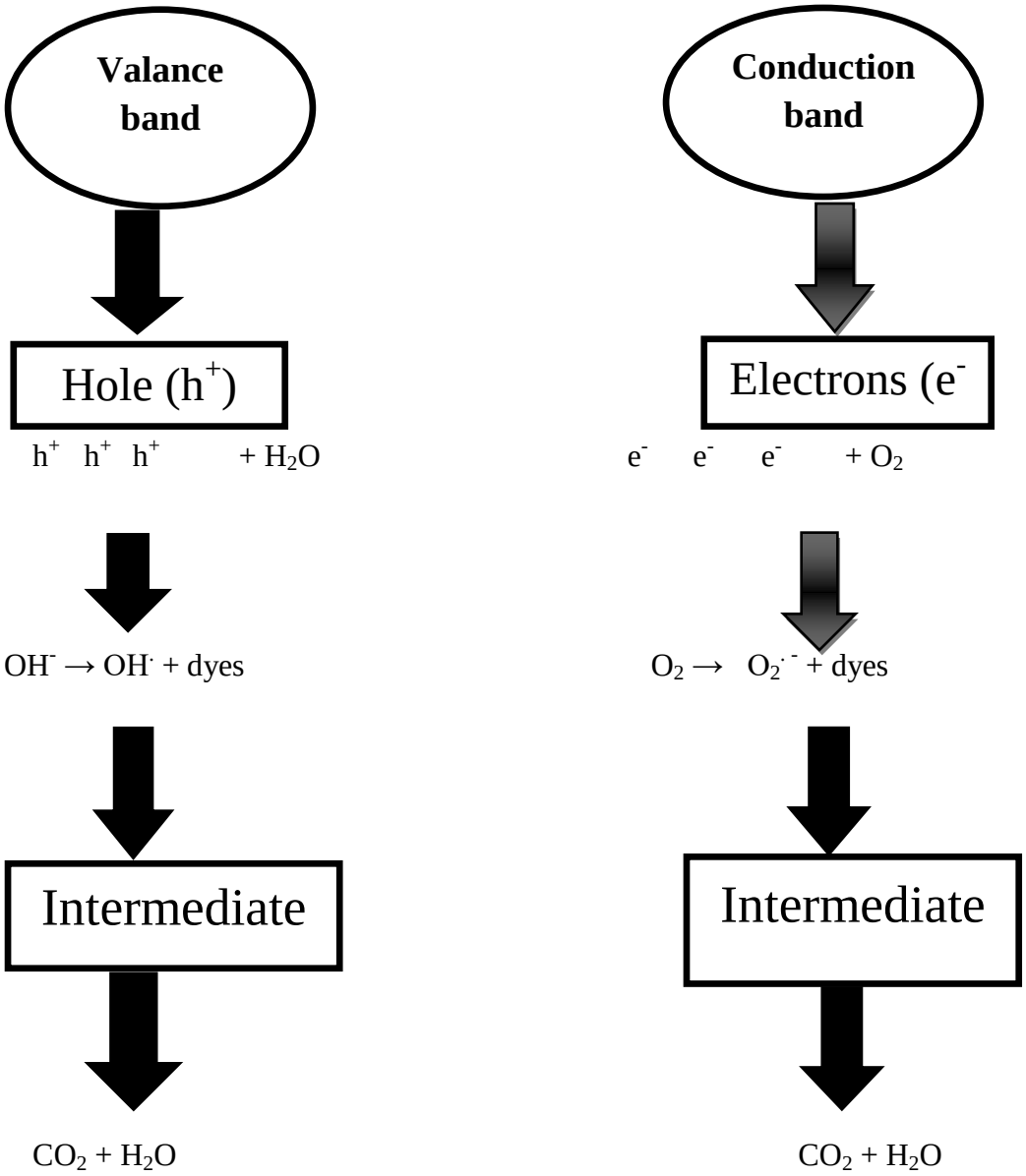

Scheme 1: Various steps in photocatalytic degradation of dyes

3. MATERIALS AND METHODS

3.1. Materials

Graphite powder was commercially obtained from Bay Carbon Company (USA). All chemicals were used as received without further purification. Hydrochloric acid (HCl; 37%, Labserv Pronalys, Australia), Sulphuric acid (H_2SO_4; 98%, Aldrich), Hydrogen peroxide (30%, German), Potassium permanganate (AR, 98%), Copper nitrate trihydrate ($Cu(NO_3)_2.3H_2O$; 99%, Alfa Aesar, India), Sodium hydroxide (NaOH; 99%, Sigma-Aldrich, India), Ascorbic acid (RG, Sigma-Aldrich) and Ethanol (99%, India), Methylene Blue (Sigma-Aldrich, >99%) were used in the experiments.

3.2. Instruments and Equipments

Ultraviolet-visible (UV-Vis) spectroscopy (Analytic Jena, Germany) was used to quantify MB. And, Fourier transform infrared (FT-IR) spectrometry (Nicolet IS10 (Thermo Scientific, Japan), X-ray diffraction (XRD) spectroscopy (XPERT-PRO, Netherlands), Scanning electron microscopy (SEM) (XL-300, USA) techniques were involved to characterize the synthesized photocatalyst. Equipments including Oven, Digital balance, Hot Plate, Magnetic bar, Centrifuge, Beakers, Test tubes, Droppers, Graduated cylinders, Glass rode, pH meter, Cuvettes, Refrigerator, Erlenmeyer flask., Furnace have been also used.

3.3. Synthesis of Graphene Oxide (GO)

The graphene oxide (GO) was synthesized from natural graphite powder according to the literature [87]. In brief, 2.0 g of graphite powder and 2.0 g of $NaNO_3$ were added into 92 mL of ice-cooled concentrated H_2SO_4(98%). Next, $KMNO_4$ (12 g) was added slowly to the solution while maintaining the reaction temperature below 20 °C. After that, the reaction was allowed to proceed in a 35 °C water bath for 2 h and 184 mL of distilled water was gradually added into it. Then, the temperature of the water bath was increased to 98 °C. The reaction was maintained at this temperature for 30 min, to increase the oxidation degree of the product. The suspension was further diluted to 1000 mL with doubly distilled water and 40 mL of H_2O_2 was added while the color of the suspension changed from brown to yellow. The product was then washed with a 5% HCl aqueous solution until the sulfate ions are removed completely. The washing process was carried out repeatedly by centrifugation at 4000 rpm for 30 min, and the supernatant was decanted away. The pH of the collected material was checked using a universal indicator. The collected material (GO) was dried under vacuum at 60 °C for 24 h.

The following equation is assumed by the reaction of $KMnO_4$ and H_2SO_4

$$2KMnO_4 + 2H_2SO_4 \longrightarrow Mn_2O_7 + H_2O + 2KHSO_4 \qquad (1)$$

The formation of more reactive Mn_2O_7 was certainly helped oxidize graphite powder as proposed in the reaction below [88].

$$Mn_2O_7 + H_2SO_4 + C(\text{graphite}) \longrightarrow \begin{pmatrix} \text{C-O-C} \\ \text{C-OH} \\ \text{COOH} \end{pmatrix} + MnO_5 + H_2O + SO4^{2-} \qquad (3)$$

3.3.1. Synthesis of Cu_2O/graphene Nanocomposite

In a typical procedure, 0.3991 g $Cu(NO_3)_2.3H_2O$ was dissolved in distilled water (30 mL) under constant stirring at room temperature, and 30 mL of GO aqueous dispersion (containing 0.05 g GO) was added into the above solution and stirred for 30 min. Then, 40 mL of NaOH aqueous solution (0.2 M) and 20 mL of ascorbic acid aqueous solution (0.1 M) were successively added into the solution. The resultant solution was placed on a heater at 70 °C for 2 h until solvent evaporation and obtaining gel state. The gel was placed in a vacuum oven for 4 h at 60 °C. Finally, the powder was calcined at 250 °C for 2 h. For comparison, Cu_2O nanoparticles were prepared by the same procedure without the presence of GO [61,73].

3.4. Characterizations of the Synthesized Cu_2O/graphene Nanocomposite

The surface morphology of the prepared products was characterized by scanning electron microscopy (SEM) (XL-300, USA) operated at 15 kV. To identify the vibrational modes of the nanocomposites, Fourier transform infrared spectroscopy (FTIR) (Nicolet IS10 (Thermo Scientific, Japan) was performed in attenuated total reflectance (ATR) mode, using a PerkinElmer Spectrum and considering 4 scans, with a resolution of $4cm^{-1}$. The optical absorption spectra of photocatalysts were estimated by Ultraviolet-visible (UV-Vis) spectroscopy (Analytic Jena, Germany) in the liquid state, and the band gaps were calculated. The crystalline of the sample was investigated by X-ray diffraction (XRD) (Almelo, Netherlands) with Cu Ka (0.15406 nm) radiation over a scan rate of $0.02^{\circ}\ s^{-1}$ at a 2 θ range of 10-70° under 40 kV/ 30 mA, at room temperature [61-66].

3.5. Photocatalytic Degradation of Methylene Blue Dye

The photocatalytic degradation of 15mg/L aqueous solutions of MB was tested using the prepared photocatalysts in visible light (200 W LED lamps) irradiation at room temperature. Here, the reaction setup was kept in a sealed Pyrex glass vessel with an unwrapped head and the light source was 10 cm apart from the reaction setup. In the process, 70 mg photocatalyst was dispersed in a 100 mL aqueous solution of MB dye (15 mg/L) in a Pyrex beaker. The solution was stirred for 40 minutes without light. This was to make sure that adsorption-desorption equilibrium was attained between the catalysts and dye solution. Then, the solution was exposed to visible light irradiation under magnetic stirring. During photocatalytic degradation, 3 mL of solution was taken at different time intervals of irradiation (30 min, 60 min, 90 min, 120 min, 150 min, and 180 min) and centrifuged to remove the precipitate. Finally, the clear liquid was measured by a UV-Vis spectrophotometer at 665 nm to measure the photodegradation efficiency [13,19]. Photodegradation was performed in the presence of 15 ppm MB solution using Cu_2O, and Cu_2O/graphene. For reference, the MB was irradiated in the absence of catalyst and their absorptions were noted.

The degradation efficiency of MB was determined by using the equation shown below [90]:

$$\text{Photodegradation efficiency (\%)} = \left[\left(\frac{Co-Ct}{Co}\right) \times 100\right] = \left[\left(\frac{Ao-At}{Ao}\right) \times 100\right] \quad (3)$$

Where C_0 is the initial concentration of MB, C_t is the concentration of MB at a time, t and A_0 is the initial absorbance of MB, A_t is the absorbance after time t light irradiation.

3.6. Parameter Optimization in Photocatalytic Degradation of MB Dye

The effect of different parameters such as contact time, catalyst dosage, and effect pH on the degradation of MB were optimized according to these literature [84,85,86].

3.6.1 Effect of contact time

The influence of irradiation time on photodegradation of MB was investigated from 30-210 min by keeping other parameters constant.

3.6.2 Effect of photocatalysts dose

The effect of catalyst amount on the degradation of MB was studied from 0.03-0.09 g of Cu_2O/graphene nanocomposite at MB solution (15 mg/L), and a reaction time of 180 min to acquire an optimized amount of photocatalyst.

3.6.3 Effect of pH

The effect of pH on the degradation of MB was investigated over a pH range of (6-11) under the optimized conditions (catalyst dose of 0.07 g of Cu_2O/graphene nanocomposite, MB solution (15 mg/L), and reaction time of 180 min. The solution was adjusted with 0.1 M HCl and 0.1 M NaOH solution to a required pH value.

3.7. Recyclability Experiments

Consecutive degradation reactions were conducted to investigate the stability and reusability of the Cu_2O/graphene nanocomposite. For these experiments, the same dose of composite sample was utilized in three consecutive cycles of photodegradation experiments. The experimental conditions were set as follows: catalyst dosage (0.7 g/L); solution volume (100 mL); initial MB concentration (15.0 mg/L); pH (10.0); and reaction time (180 min.). The composite was recovered by centrifugation after each reaction, purified with distilled water, and dried under vacuum (60 °C, overnight). Then, it was reused in another reaction.

4. RESULTS AND DISCUSSION

4.1 Graphene Oxide Formation

Graphene oxide was prepared from graphite through one-pot synthesis based on newly modified Hummer's method [87]. The oxidation of graphite by concentrated H_2SO_4/$NaNO_3$ and $KMnO_4$ results in a greenish dark paste (Fig. 3a). The dark green color could indicate Mn_2O_7 formation. The mixture was stirred for 2 h at 35 °C and its color changed to a brown paste which could indicate an oxidation process has occurred (Fig. 3b). After adding distilled water into the mixture, no purple color was shown which indicated $KMnO_4$ is fully reacted [94]. The addition of H_2O_2 into the mixture also released heat and effervesces (evolution of steam and oxygen gas) (Fig.3c), and a bright yellow color was observed (Fig. 3d). The purpose of H_2O_2 was to consume the residue of $KMnO_4$ [95]. The color change possibly is due to the high-level oxidation of graphite powder, as reported in the literature [96]. The dispersion of the product in H_2O upon the mechanical stirring is due to the introduction of functional groups which are responsible for the hydrophilic nature of graphite oxide. The filtration of the mixture resulted in a brown paste, which confirms the formation of graphite oxide. The washing process of graphite oxide paste with 5% HCl aqueous solution was done using centrifuge until SO_4^{2-} was removed.

Generally, the preparation of GO and graphene had three stages; (1) Low-temperature stage, in this stage the mixture of graphite, $NaNO_3$, $KMnO_4$, and H_2SO_4 was deep green (Fig. 3a). (2) Medium-temperature stage, in this stage the deep green color changed to brown (Fig. 3b). (3) High-temperature stage, the brawn colure changed to a yellow solution when after H_2O_2 was added (Fig. 3d).

The reduction of GO was also monitored by visual observation. As shown in Fig. 3(e), the GO dispersion resulted in brownish yellow color while the reduction of GO with ascorbic acid resulted in a black dispersion (Fig. 3f). This was probably a result of an increase in the hydrophobicity of the material caused by a decrease in oxygen-containing functional groups (O-H, C-OH, COOH, and C-O) on the surface of the sheets [97]. The color change or the black color of graphene can also be assigned to the partial restoration of the π-network between the sheets due to removal of oxygen containing functional groups resulted in electronic conjugation with in reduced sheets [91,92].

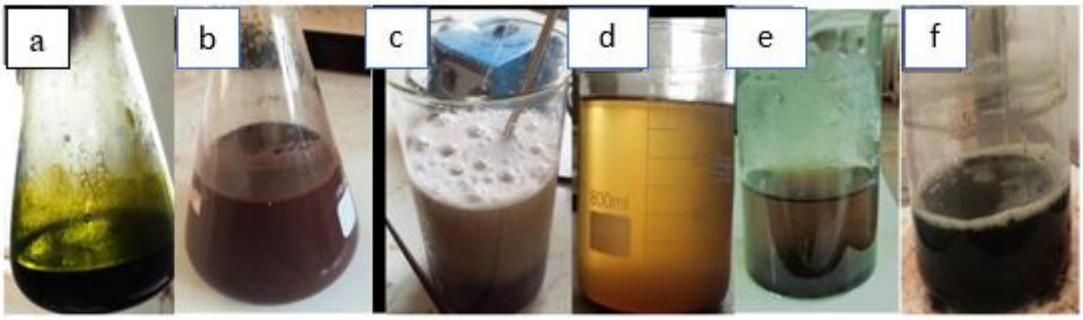

Figure 3. Schematic illustrations of color observations during the oxidation of graphite.

4.1.1 Cu_2O/graphene Nanocomposite Preparation

A facile sol-gel process is introduced to prepare the Cu_2O/graphene nanocomposite in which both the formation of Cu_2O nanoparticles and the reduction of GO are achieved in a one-pot reaction. It is reported that the exteriors of the chemically exfoliated GO sheets are wrapped up by a large number of hydroxyls, carboxyl and epoxy groups which are brought in on GO sheets during oxidation [100]. These functional groups are responsible for the tie-up of Cu $(OH)_2$ crystals onto GO sheets which enables the subsequent in situ formation of nanoparticles and the simultaneous reduction to Graphene using ascorbic acid in the reaction medium. After the mixing of the GO suspension and $Cu(NO_3)_2$ solution, Cu^{+2} ions are adsorbed onto the GO surfaces due to the bonding with the oxygen atoms of the negatively charged oxygen-containing functional groups via electrostatic forces[101]. The addition of NaOH not only increases the pH of the reaction medium but also helps to generate Cu $(OH)_2$ crystals which act as precursors for Cu_2O nanoparticles. This Cu $(OH)_2$ crystals tie up with the functional groups of GO via intermolecular hydrogen bonding or coordination bonds as shown by equation(5) [102]. Finally, ascorbic acid reduces the Cu $(OH)_2$ to produce Cu_2O nanoparticles. Meanwhile, Graphene sheets are formed through the reduction of GO as shown by equation (6). Thus, the Cu_2O/graphene nanocomposite was obtained from both of the reduction reactions carried out in one step under heating at 70 °C.

$$Cu(NO_3)_2.3H_2O + NaOH + GO \longrightarrow Cu(OH)_2/GO + NaNO_3 + H_2O \quad (5)$$

$$Cu(OH)_2/GO + \text{ascorbic acid} \longrightarrow Cu_2O/\text{graphene} \quad (6)$$

4.2 Characterization of Cu_2O/graphene Nanocomposite

4.2.1 Parameters Optimization for the Synthesis of Cu_2O/graphene Nanocomposites

4.2.1.1 Effect of GO Amount

To investigate the influence of GO amount in the synthesis of Cu_2O/graphene nanocomposite, amount of GO was varied from (0.01-0.08wt %) and its light-absorbance property was probed with UV-visible (UV-Vis) spectroscopy. As depicted in (appendix 1), the absorption edge of Cu_2O/0.01wt% GO as well as Cu_2O/0.05wt% GO kindly shifts to the visible light range. Additionally, it is noteworthy that Cu_2O/0.08wt% GO shows a weaker absorbance than that of Cu_2O/0.01wt% GO and Cu_2O/0.05wt% GO in the visible light region. In addition, the influences of different mass ratio of GO on MB photodegradation was performed. The result showed that, along with the increase of GO content, the photocatalytic activity of the Cu_2O/graphene composites is at first increased and then decreased. When the GO content in the composite reaches 0.05 wt%, the amount of MB degraded was enhanced. The enhancement of the photocatalytic activity for MB degradation could be attributed to the excellent electronic conductivity and large specific surface area of Graphene [103], resulting in that the photogenerated electrons transport to the surface of the composites more easily, thus inhibiting the recombination between photoinduced electrons and holes.

4.2.1.2 Effect of Temperature

Temperature is one of the key influence factors in chemical reactions. To investigate the influence of heating in the synthesis of Cu_2O/graphene nanocomposite, the solution temperature was heated at 60, 70, and 80 °C, while other parameters were kept constant. In (appendix 2), the UV-Vis spectra of Cu_2O/graphene generated at different reaction temperatures, all in aqueous suspension are presented. It can be observed that as the reaction temperature increases the Cu_2O/graphene peak absorption is also shifted (λ_{60}= 466 nm; λ_{70}=511 nm; λ_{80}=477 nm). For 60 and 80 °C, the absorption spectra show broad and unsymmetrical band peaks, which indicate that NPs size distribution is broad and that probably they are aggregated [104,105]. For 70 °C, the absorption band peak, in this case, is narrow and very symmetrical that indicates the formation of more intense phases of Cu_2O nanoparticles. Hence particle size is homogeneous and particles are very well dispersed [98].

4.2.1.3 Effect of Reaction Time

The quality and type of nanocomposite synthesized were greatly influenced by the length of time for which the reaction medium is incubated. Contact time is one of the parameters that control the size of Cu_2O/graphene nanocomposite because of the blue shift of the absorption peaks as shown in (appendix 3). It can be seen that at 1 h, the band is broadened because of the slow conversion of copper ion (Cu^{2+}) to zerovalent copper (Cu^0) nanoparticles. Increasing the contact time enhances excellent band formation because a large amount of Cu^{2+} has been converted to Cu^0 [106]. However, further increase in contact time leads to a noticeable decrease in absorption intensity and wavelength which is an indication of some aggregation of Cu_2O/graphene nanocomposite due to long time reaction; particles may shrink or grow during the long reaction; they may have a shelf life, and so forth, that affects their potential [107].

4.2.2 UV-Vis spectroscopy Analysis

To demonstrate the effect of the presence of graphene on the photo-response of the prepared Cu_2O/graphene nanocomposite, UV–Vis absorption spectroscopy was performed on the samples. As depicted in Fig.4 the UV–Vis spectrum of GO exhibits a maximum absorption peak at about 234 nm, corresponding to the π-π^* transition of aromatic C=C bonds [96,97] and the shoulder peak at 300 nm corresponding to the n-π^* transitions of C=O bond from oxidized carbon of GO [94,98]. The overall feature of this spectrum is comparable to that of the GO synthesized using different methods and its adsorption peaks are also similar to those of the GO samples reported in the literature [111].

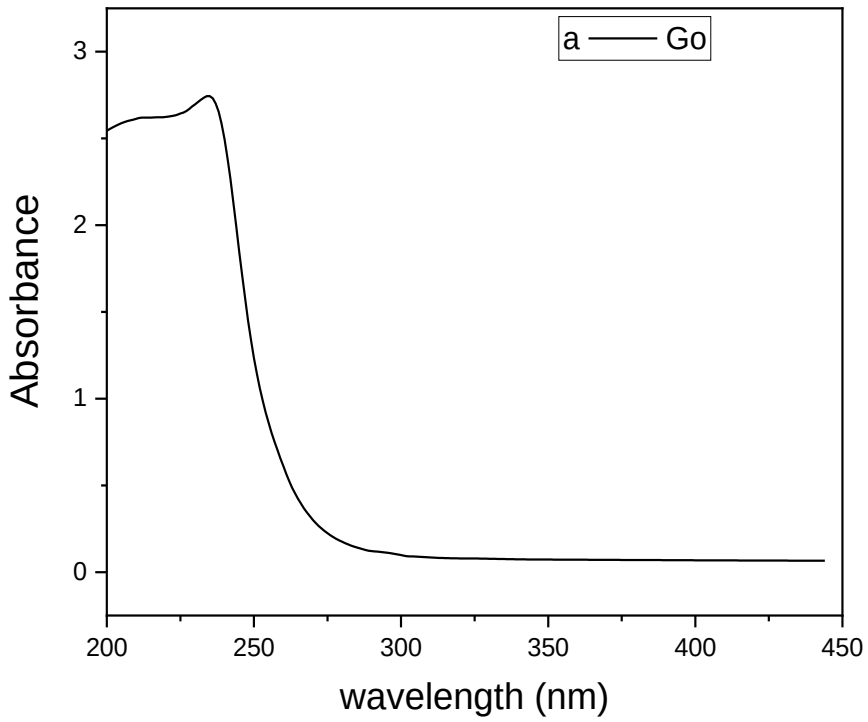

Figure 4. UV visible spectroscopy absorption spectra of GO

A broad absorption band located at 484 nm attributes the formation of cubic crystals of Cu_2O to the chemical reaction between the $Cu(NO_3)_2.3H_2O$ and ascorbic acid solution. However, Cu_2O/graphene nanocomposites showed enhanced absorption in the long-wavelength region ranging about 500 nm as indicated in Fig. 5(c). The increase of absorption in the visible light region is due to the reintroduction of graphene, which can be ascribed to the increase of surface electric charge of Cu_2O in the composites and restrain the recombination of electronic–hole pairs [112].

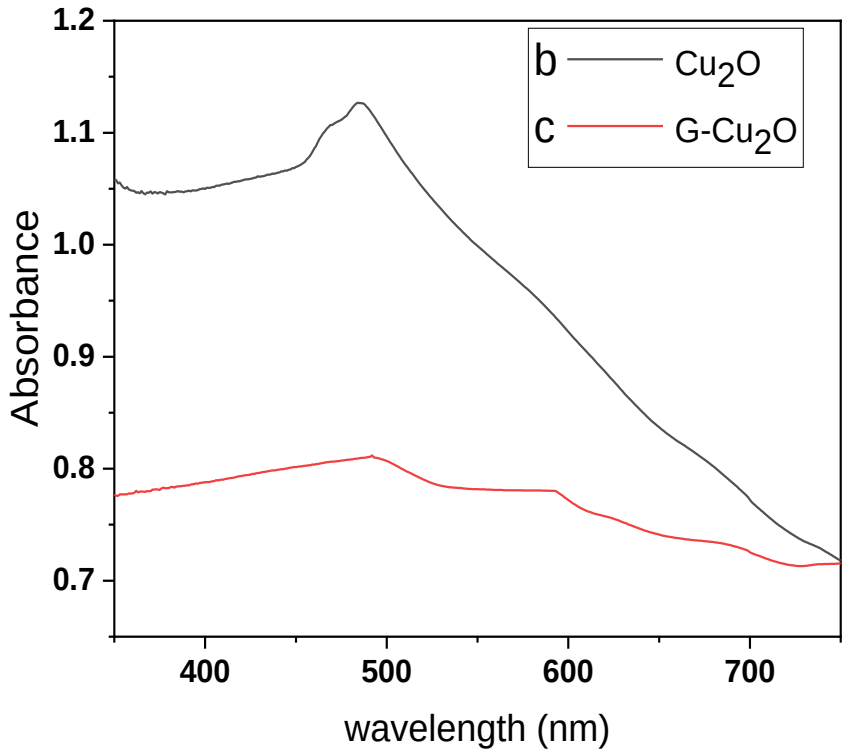

Figure 5. UV visible spectroscopy absorption spectra of Cu_2O, and Cu_2O/graphene nanocomposite synthesized at (70 ^oC, and 2h).

The optical band gaps of the synthesized materials were calculated by using Tauc's equation (6) [113]:

$$\alpha h\nu = A(h\nu - E_g)^{n/2} \qquad (6)$$

Where α is the absorption coefficient, E_g is the band gap, A is a constant, and n is an index that characterizes the optical absorption process (for direct band gap semiconductor material $n = {}^1/_2$ and for indirect transition n=2). By extrapolating the linear region of the plot $(\alpha h\nu)^2$ vs. $h\nu$, the band gap could be estimated. The bandgap values for Cu_2O and Cu_2O/graphene are given in Fig. 6. As depicted in Fig. 6(a, and b) the band gap of Cu_2O/graphene nanocomposite (1.96 eV) is smaller than that of synthesized Cu_2O (2.03 eV) nanoparticles. This indicates, graphene played an essential role in the band gap energy reduction of Cu_2O nanoparticles.

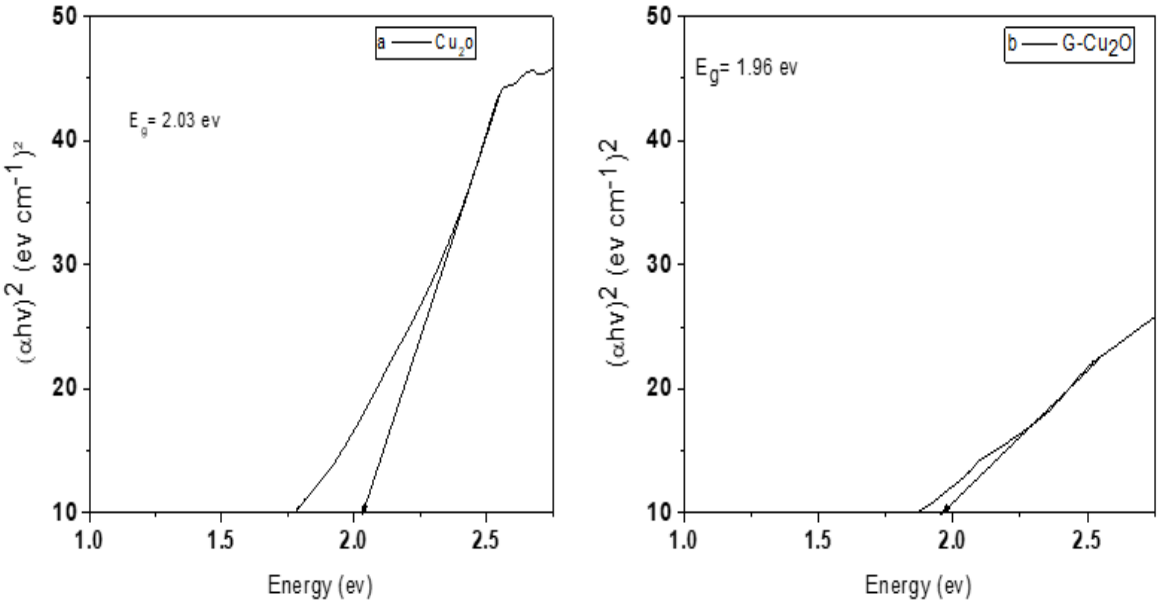

Figure 6. Energy band gap of (a) Cu_2O, and (b) Cu_2O/graphene nanocomposite

4.3 XRD Analysis

The crystalline and amorphous nature of Cu_2O and Cu_2O/graphene nanocomposites were examined using XRD patterns as shown in Fig.7. The peaks at 29.74°, 36.58°, 42.49°, 55.10°, 61.62, and 65.91°, which were attributed to the (110), (111), (200), (211), (220), and (221) planes for pure Cu_2O nanoparticles. The intensities and positions of the diffraction peaks closely resemble the reference patterns for the cubic phase of Cu_2O (Joint Committee for Powder Diffraction Studies (JCPDS) card no. 05-0667) [102]. The d-spacing was calculated as 0.24 nm with respect to plane (111) in Cu_2O nanoparticles. But, the peaks at 32.28° do not fit well with Cu_2O particles and confirm the existence of other Cu-O phases like CuO [114]. The peaks that appeared in Cu_2O/graphene nanocomposite also exhibit comparable diffraction peaks and confirm the presence of Cu_2O in the composite. The (111) peak of nanocomposites is relatively narrower than that of pure Cu_2O nanoparticles which is due to the distortion in the lattice structure of Cu_2O by the interaction with graphene sheets. The sharp intensity of diffraction peaks of pure Cu_2O nanoparticles and Cu_2O/graphene nanocomposites indicate that the synthesized samples have high crystallinity.

The crystallite size of Cu_2O nanoparticles and Cu_2O/graphene nanocomposite was calculated using the most intense peaks and found to be about 28.6 and 23.3 nm respectively using the Debye Scherer equation given below[115].

$$D = \frac{0.9\,\lambda}{\beta \cos\theta}$$

Where D is particle size, λ is the wavelength of the X-rays = 0.154 nm, β is the full width at half maximum of two most intense XRD peaks, in this case, K is Scherer constant (K =0.9), and θ is the Bragg diffraction angle.

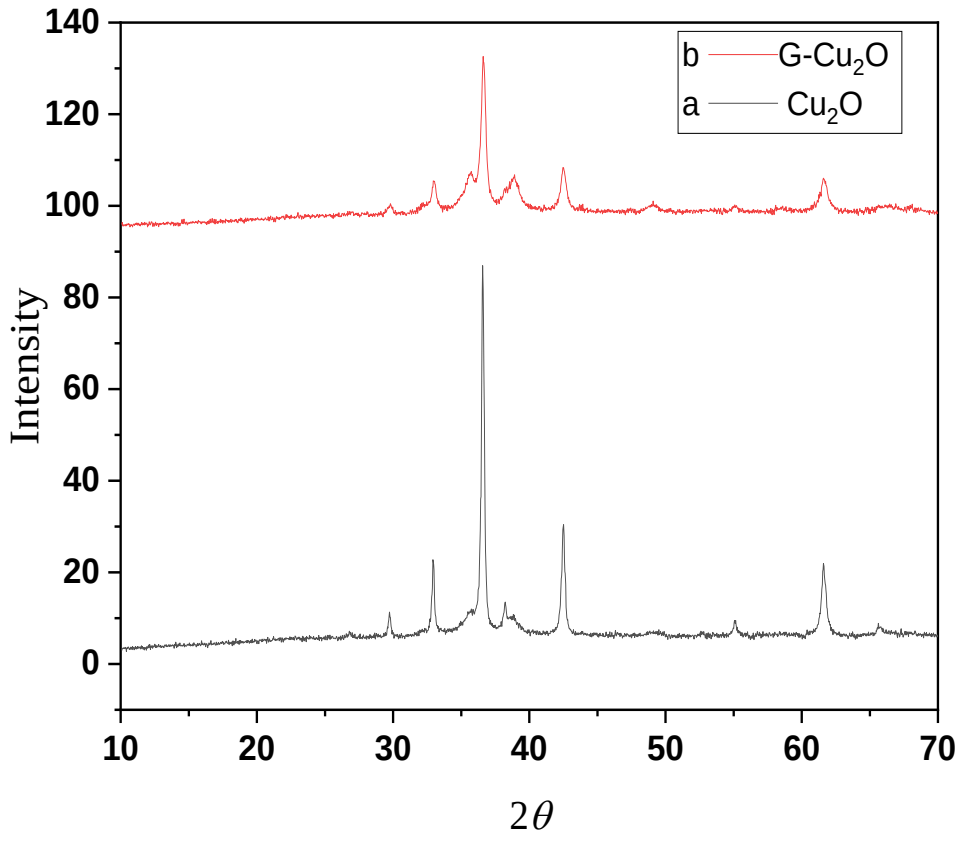

Figure 7. XRD patterns of (a) Cu_2O, and (b) Cu_2O/graphene nanocomposite synthesized at (70 ^oC, and 2h)

4.4 SEM Analysis

The morphologies of the synthesized Cu_2O nanoparticles and Cu_2O/graphene composite were characterized by using scanning electron microscopy (SEM). The SEM image (Fig. 8a) shows that the shapes of the Cu_2O nanoparticles appeared spherical and its surface is not smooth. In addition, the particles are agglomerated. The SEM image of Cu_2O/graphene nanocomposite (Fig. 8b) shows that the Cu_2O is covering on the basal plane of the graphene within high homogeneity and low aggregation[116].

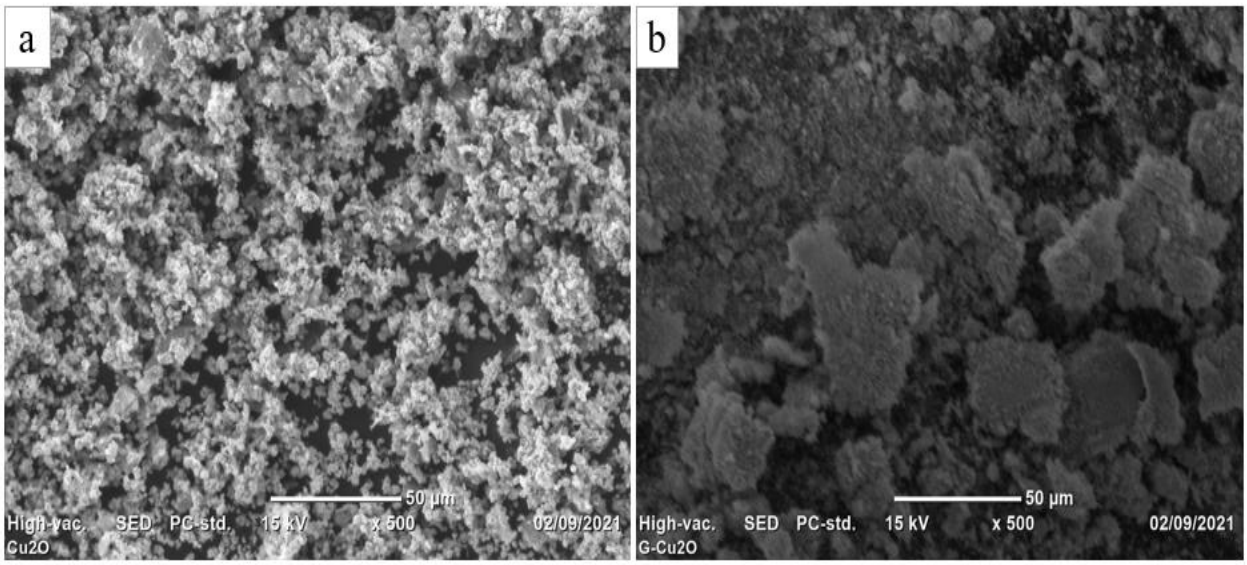

Figure 8. SEM images of (a) Cu_2O and (b) Cu_2O/graphene nanocomposites synthesized at (70 ^oC, and 2h)

4.5 Fourier Transform Infrared Spectroscopy (FTIR)

FTIR was used to identify functional groups of the prepared nanomaterials. Fig. 9 shows FTIR of GO, Cu_2O, and Cu_2O/graphene nanocomposite. GO displayed abundant oxygen-containing groups, the strong band at around 3405 cm^{-1} is due to the stretching vibration of O-H, the band at 1734 cm^{-1} indicates the C=O vibration of -COOH located at the edge of GO sheets [97]. The peaks at 2924 cm^{-1} occurred due to C-H stretch vibrations. The deformation peak of O-H of C–OH group) and Alkenyl C=C stretching peak can be seen at 1452 and 1616 cm^{-1} respectively [117]. The peak at 1372 cm^{-1} is attributed to the tertiary C-OH groups stretching vibration, the band at 1164 cm^{-1} is referred to as aromatic C-H bond [21], and the band at 1040 cm^{-1} is due to C-O stretching vibration of C-O-C. All of the characteristic vibration bands are indicative of the containing of hydroxyl, carboxyl, epoxide groups in GO.

On the other hand, the Cu_2O displays an intense peak at 626 cm^{-1}, which is attributed to Cu-O vibration, the other two peaks located at 3404 and 1610 cm^{-1} are caused by the stretching and bending vibrations of hydroxyl groups of the inevitably adsorbed water [118]. In the FTIR spectra of Cu_2O/graphene nanocomposite, the intensities of the oxygen-containing groups significantly decreased due to the reduction of GO by ascorbic acid while the peak at 2951 and 2360 cm^{-1} which corresponds to C-H stretch vibrations and the adsorbed CO_2 [118,119] respectively. In addition, the Cu-O vibration of Cu_2O shifts slightly to 536 cm^{-1}, indicating the interaction between Cu_2O and graphene perturbing the Cu-O bonds [22].

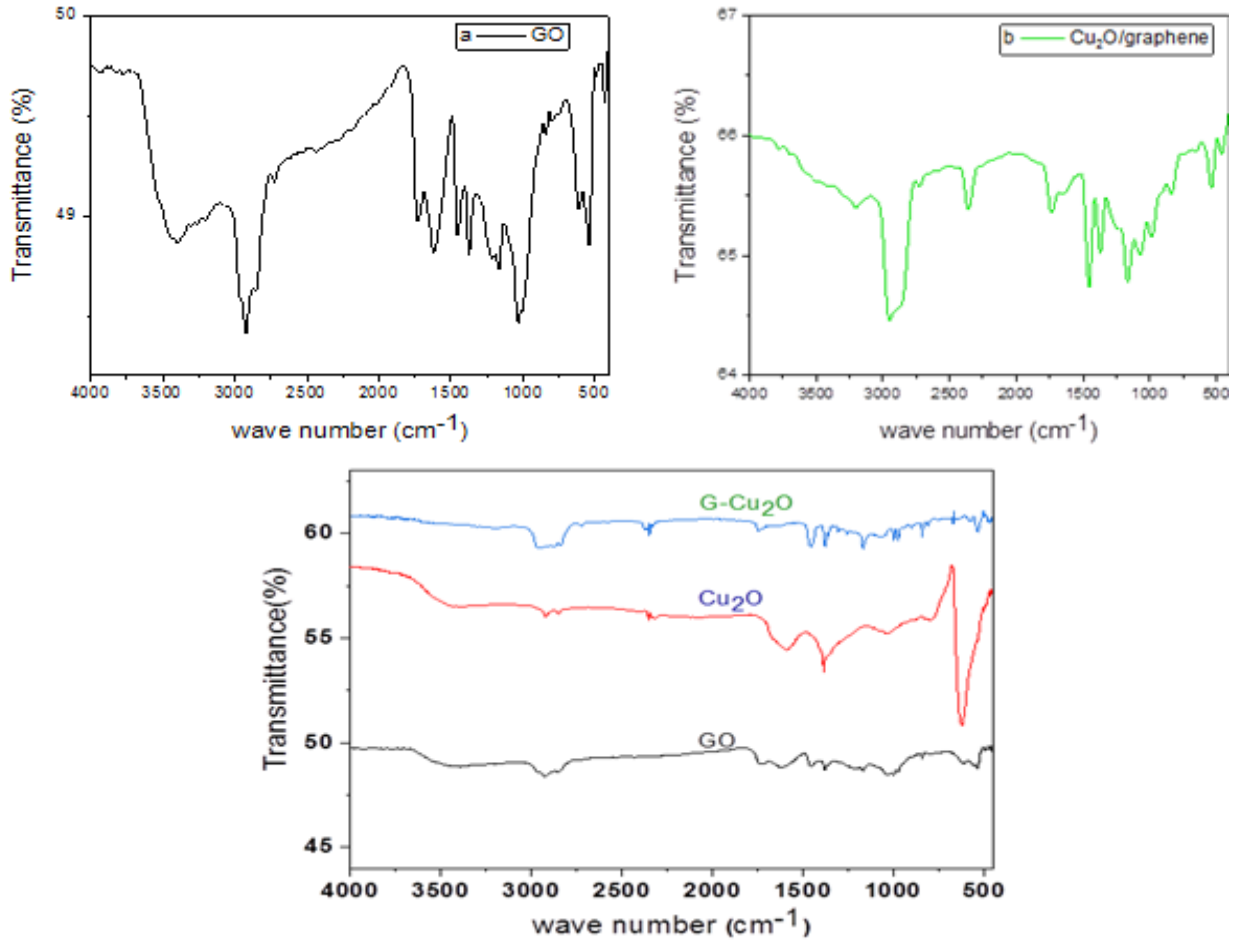

Figure 9. FT-IR spectra of GO, Cu_2O, and Cu_2O/graphene nanocomposite synthesized at (70 ^oC, and 2h).

4.6 Application of the Synthesized Nanocomposite

4.6.1 Optimization of Photocatalytic Degradation of MB dye

4.6.1.1 Effect of Contact Time

The effect of contact time on the photodegradation of MB has been studied in presence of Cu_2O/graphene nanocomposite under visible light (Fig. 10). The result showed that the degradation efficiency (82%) was increased as time increased. This is because the interaction of dye molecules increased with the surface of the photocatalyst. The maximum degradation efficiency was observed at 180 min because above it there is negligible degradation efficiency change was observed. Hence, 180 min. was considered in the follow up experiments.

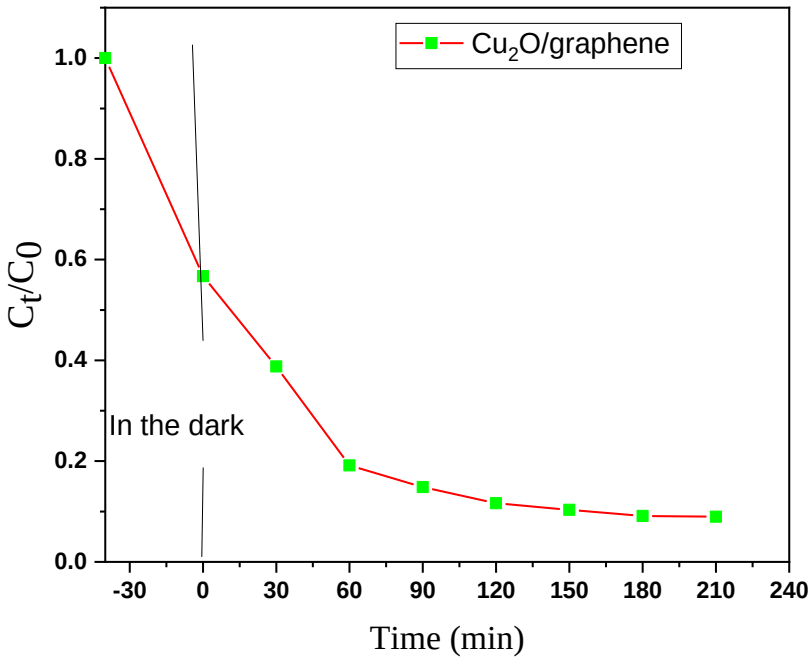

Figure 10. Effect of irradiation time on photocatalytic degradation of MB with Cu_2O/graphene nanocomposite under varying contact time

4.6.1.2 Effect of Catalyst Dose

Photocatalytic degradation is affected by the amount of catalyst. Hence the amount of catalyst is a key parameter during the suspended photodegradation reactions. The effect of Cu_2O/graphene dosage on MB photodegradation was investigated by various amounts of the composite photocatalysts (0.3, 0.5, 0.7, and 0.9 g/L) under the condition of 100 mL MB solution of 15 mg/L, and irradiation time 180 min. As shown in Fig. 11, when the photocatalyst amount increases from 0.3 to 0.7 g/L, MB degradation increases from11.1% to 84% after 180 min of irradiation. This improvement of the removal rate is caused by the number of active sites on the catalyst surface being increased as the photocatalyst dosage increases, resulting in the increment of the amount of superoxide and hydroxyl radicals [121] and the collision frequency between the catalyst and dye increases [122]. However, the MB degradation decreases to 78% with a further increase in photocatalyst amount to 0.9 g/L. This is due to an agglomeration and sedimentation of the catalyst particles which caused an increase in the particle size that lead to a decrease in the number of surface active sites on photocatalyst surface [123]. Also, at a high amount of catalyst, the opacity, turbidity of the suspension, and light scattering of catalyst particles are increased. This tends to decrease the passage of irradiation through the sample [116,117]. Therefore, the optimal photocatalyst amount of 0.7 g/L is employed for the optimization of the other photodegradation parameters.

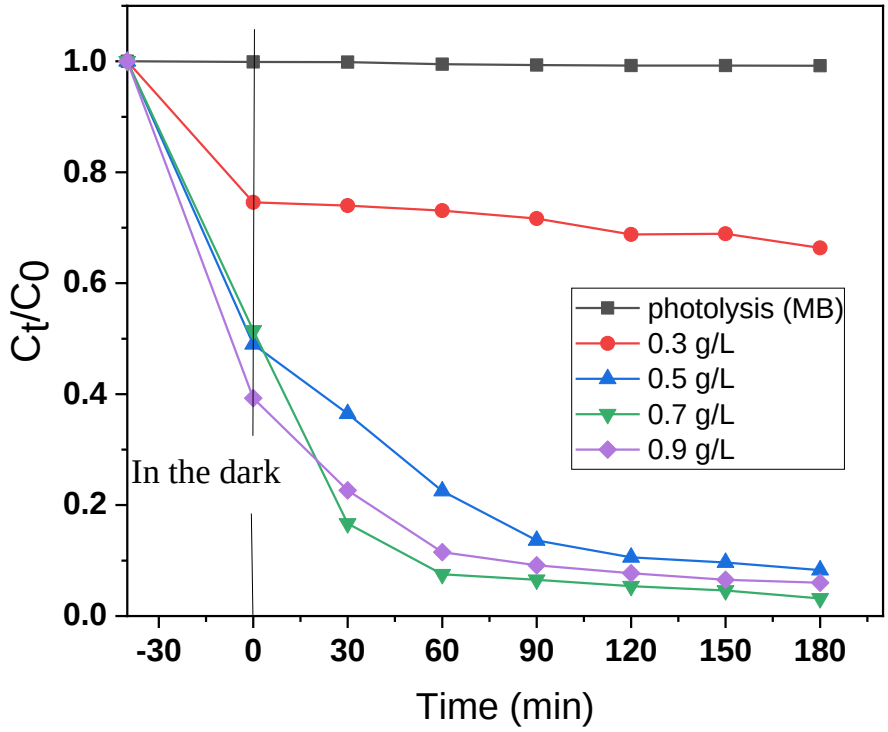

Figure 11. Effect of catalyst on the degradation of MB at 15 mg/L of MB, and irradiation time 180 min

4.6.1.3 Effect of pH

The solution pH is an important parameter that influences the rate of photocatalytic degradation of some organic compounds. The effect of pH on the photodegradation the efficiency of MB was investigated from 6-11 in the presence of a fixed amount of catalyst (0.7 g/L), 100 mL of 15 mg/L dye solution, and irradiation time 180 min. Fig. 12 demonstrates the results of photodegradation efficiency of MB with different pH values. Also, the point of zero charges of Cu_2O/graphene nanocomposite is 7.6 as depicted in appendix 5. The results revealed that the photodegradation efficiency increases with the increase in pH. At pH 6.0 less significant degradation was observed. It is well known that in the acidic ($pH < pH_{pzc}= 7.6$) region, the efficiency of degradation is less; this is because both the surface of the catalyst and MB are positively charged. The occurrence of desorption could be explained by electrostatic repulsion [126] between MB and Cu_2O/graphene because the surface of Cu_2O/graphene is positively charged at pH 6.0. As a result, poor adsorption of MB on the surface of Cu_2O/graphene occurred. In contrast, above the zero-point charge of Cu_2O/graphene ($pH > pH_{pzc}=7.6$), the Cu_2O/graphene surface is negatively charged and in an

aqueous solution, MB has a positive charge. Due to electrostatic interaction[127] between the negatively charged Cu_2O/graphene surface and positively charged MB dye, higher photodegradation efficiency is obtained in alkaline solution. However, with further increasing pH of the solution, repulsion of hydroxide ions by the negatively charged photocatalyst surface can lead to a reduction in OH radical formation, and hence, a decrease in photodegradation efficiency can be occurred [124, 125]. Therefore, Optimum degradation of Methylene blue dye is obtained at pH-10 which degrades the dye up to 94% under the irradiation time of 180 min.

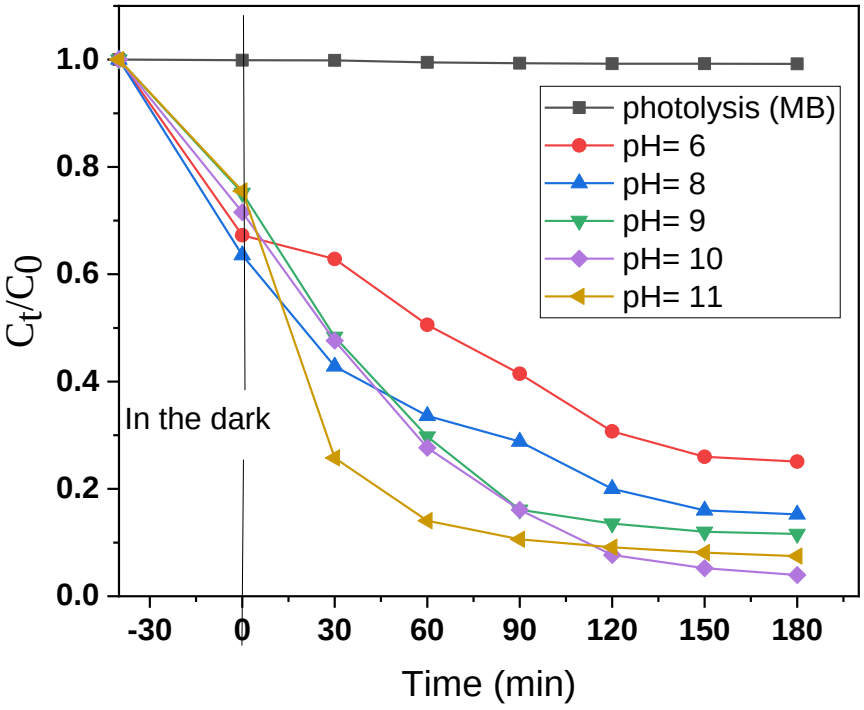

Figure 12. Effect of pH on the degradation of MB at Catalyst dose of Cu_2O/graphene 0.7 g/L, and irradiation time 180 min

4.7 Degradation of MB using Cu_2O and Cu_2O/graphene at Optimum Conditions

From the optimized parameters, the most efficient photocatalytic degradation of MB was at 0.7 g/L catalyst dosage, pH 10, and irradiation time 180 min. The results for MB degradation are shown in Fig. 13. A continuous decrease in the intensity of the characteristic absorbance band of MB dye centered at ~664 nm with increasing irradiation time reflects the photodegradation of MB dye. Cu_2O /graphene and Cu_2O nanoparticles show 94% and 67% degradation of MB solution in 180 min., respectively, showing excellent photocatalytic performance of Cu_2O/graphene in comparison with pure Cu_2O. This is due to the larger surface of graphene sheets that can offer more active adsorption sites, resulting in enhanced adsorptivity of MB molecules. Moreover, the photo-generated electrons can easily transfer to graphene, leading to enhanced charge separation, which is crucial in enhancing photocatalytic reactivity[126,127].

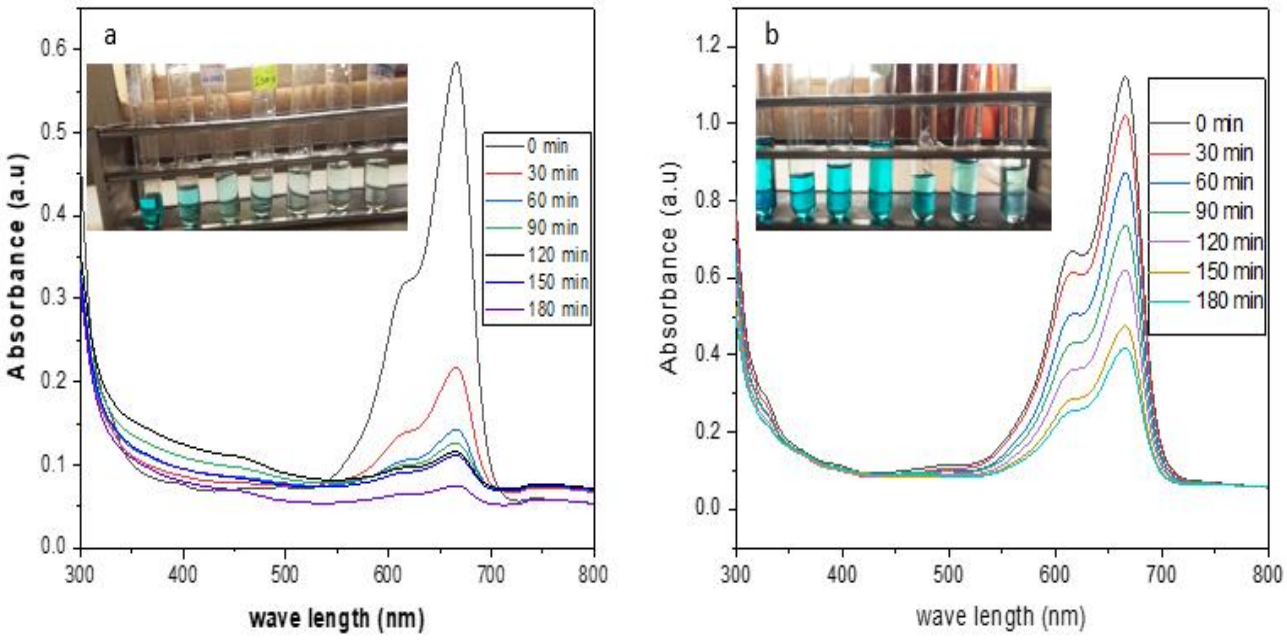

Figure 13. MB dye degradation during light irradiation in the presence of (a) Cu_2O/graphene and (b) Cu_2O at 0.7 g/L catalyst, pH-10, and irradiation time 180 min.

4.8 Kinetics Studies of the Degradation Process

Degradation kinetics was explored to further understand the degradation process. Here, the degradation efficiency of MB in the presence of a different concentration of Cu_2O/graphene composites and at various pH under visible light was evaluated by the second-order kinetic model. The photocatalytic degradation rate equation was expressed as follows [132]:

$$\frac{1}{Ct} = kt + \frac{1}{C0} \qquad (7)$$

The equation (7) is the linearized form of the second-order kinetics, where C_0 and C_t are the concentration of the organic pollutant solutions at the initial time (t=0) and reaction time (t≠0), k (min^{-1}) is the second-order rate constant, and t (min) is the reaction time. The value of the k (rate constant) can be calculated from the slope of the linear plot of $1/C_t$ as a function of t (, Fig. 14). The degradation process with different catalyst amounts and pH can be fitted well with a second-order kinetic model, as shown in (Fig. 14 a, and b). The calculated k values, as well as the determination coefficient (R^2) values for the degradation of MB at different experimental conditions, are given in Table 1. From Table 1, it can be seen that the coefficient of determination (R^2) for the second-order kinetic model is greater than 0.95 which is higher than the R^2 values of the first-order kinetic model (appendix 4). Therefore, R^2 values confirm that photocatalytic degradation is a second-order kinetic process. In addition, the calculated second-order rate constants of Cu_2O/graphene and pure Cu_2O are 0.0539 and 0.0085 $M^{-1}.min^{-1}$ respectively (Fig. 14 c). The results further demonstrated that Cu_2O/graphene photocatalyst exhibits good photo-reactivity which corroborates the corresponding degradation efficiency.

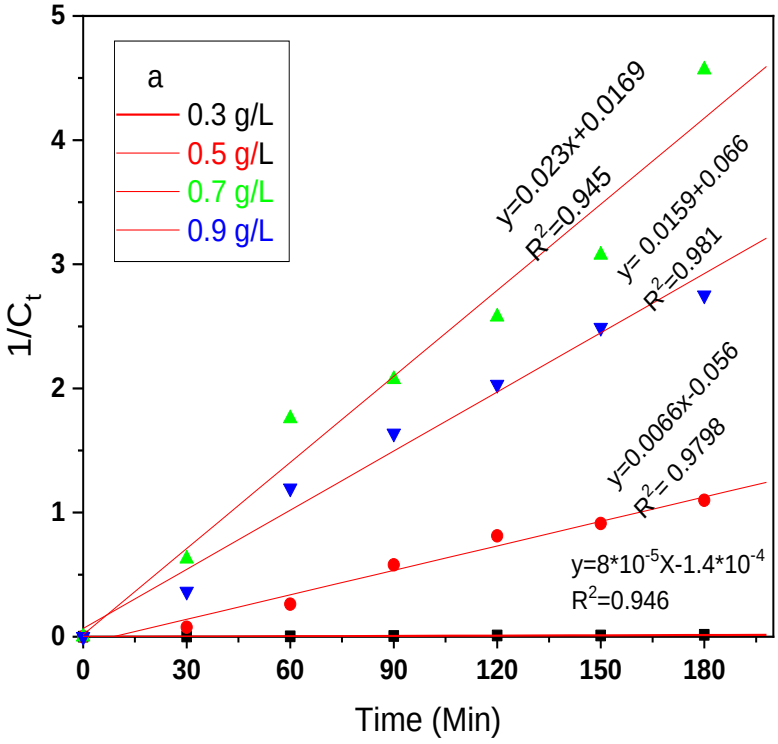
a
0.3 g/L
0.5 g/L
0.7 g/L
0.9 g/L
y=0.023x+0.0169
R2=0.945
y= 0.0159+0.066
R2=0.981
y=0.0066x-0.056
R2= 0.9798
y=8*10-5X-1.4*10-4
R2=0.946
1/Ct
Time (Min)
0
1
2
3
4
5
0
30
60
90
120
150
180

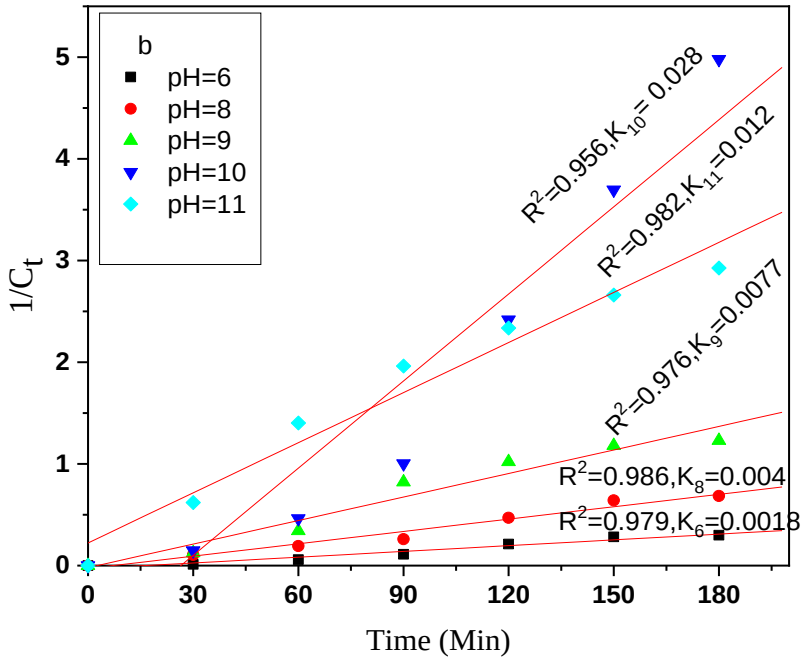

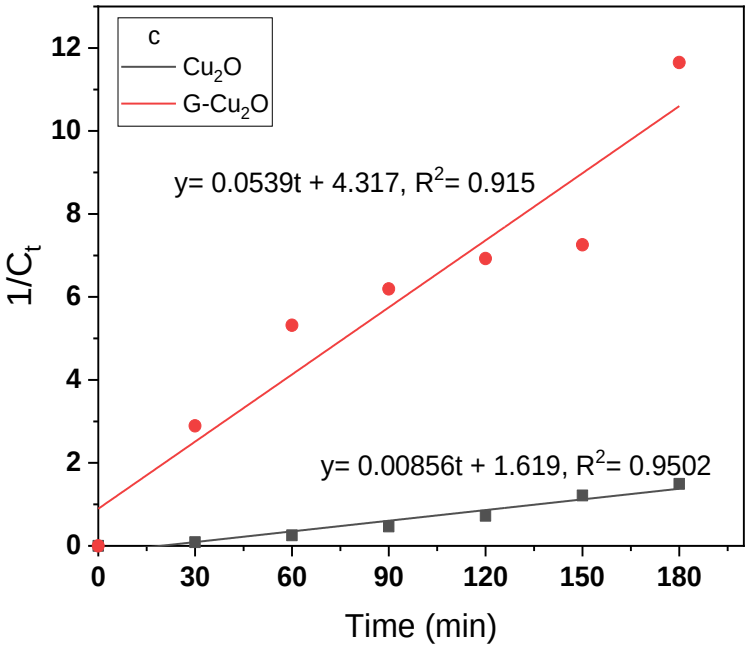

Figure 14. Second-order kinetic model for degradation of MB by (a) at different catalyst dosage (b) at various PH (c) Cu_2O/graphene and Cu_2O in reaction conditions: MB = 15 (mg/L),

Table 1. Second-order rate constants and regression coefficients were obtained at different initial Cu_2O/graphene catalyst concentrations, Cu_2O, and pH.

parameters	Amount	K($M^{-1}.min^{-1}$)	R^2
Catalyst Dosage	0.03 g	0.0008	0.946
	0.05 g	0.0066	0.979
	0.07 g	0.0159	0.981
	0.09 g	0.023	0.945
pH	6	0.0018	0.979
	8	0.004	0.986
	9	0.0077	0.976
	10	0.028	0.982
	11	0.012	0.956
Cu_2O/graphene	0.07 g	0.0539	0.914
Cu_2O	0.07 g	0.00856	0.945

4.9 Reusability of the Cu_2O/graphene Nanocomposite

The reusability of the Cu_2O/graphene nanocomposite as catalysts in the degradation of MB was investigated in consecutive cycles. The degradation capability of regenerated Cu_2O/graphene was tested under similar conditions (pH=10 and 100 mL of 15 mg/L MB) and compared to the performance of the first cycle. There is a slight decrease in the photocatalytic activity of MB during the first cycling runs (Fig.15), showing promising reusability even over third cycles. It can be the limitation of our work that, since the loss of some amount of the photocatalyst during the filtration in the repeated experiments, we were unable to repeat the experiment for several cycles. In fact, the experiment need to be repeated for several runs until the trend significantly decreased. This decrement may be explained by the deposition of organic species on active sites of catalyst, inhibiting its catalytic activity [110,111]. This indicates that the prepared photocatalysts exhibit good photocatalytic stability and reusability under visible light irradiation.

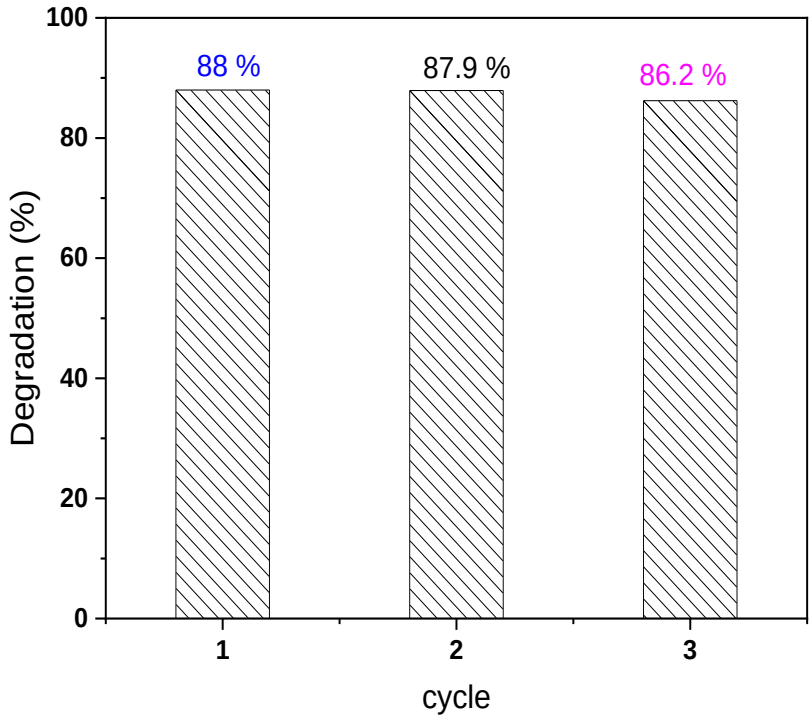

Figure 15. Reusability of Cu_2O/graphene nanocomposite (initial MB concentration: 15 mg/L, photocatalyst dosage: 0.7 g/L, pH: 10 and irradiation time 180 min).

4.10 Proposed Mechanism of Photodegradation

The photocatalytic degradation of MB occurs through several steps and the schematic of this is illustrated in Fig. 16. When an aqueous solution containing photocatalyst and contaminant molecules (here MB) is irradiated by visible light, electron-hole pairs are generated (Equation. (8). In the first step, when the semiconductor is illuminated by the light energy, the electron in the valence band absorbs energy and moves to the conduction band. The generated holes in the valence band react with H_2O molecules, resulting in the formation of hydroxyl radical ($^{\bullet}OH$) as given by Equation (10) and demonstrated in Fig. 16. The excited electrons in the conduction band react with O_2 molecules to form superoxide radical ions ($\bullet O_2^-$) (Equation (11). Finally, the hydroxyl radicals, which can oxidize and mineralize the organic molecules, react with MB molecules, which results in the production of different species, such as carbon dioxide, and water (equation (14) [123].

Moreover, the photosensitization of adsorbed MB dye will also generate the excited electrons and increase the number of active radicals $O_2^{\bullet}$. The $O_2^{\bullet}$ radical further undergoes a series of reactions and produces H_2O_2 as the intermediate which further gives hydroxyl ($OH^{\bullet}$) radicals. These $OH^{\bullet}$ radicals are therefore successfully hit the $C{-}S^+{=}C$ functional group of the dye attached to the photocatalysts and degrade the dye molecules into small fragments [135]. The visible light-driven photodegradation process of MB dye using synthesized photocatalysts can be understood by the following reaction steps.

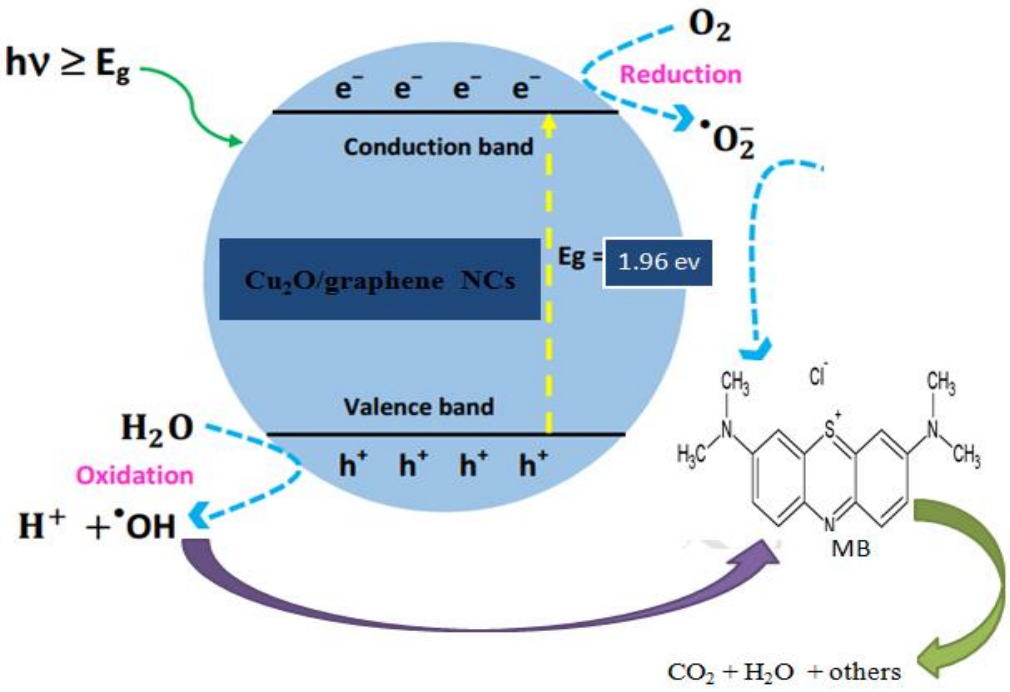

Figure 16. Schematic diagram of the charge transfer mechanism in the synthesized photocatalysts.

Cu_2O/graphene + hν ⟶ h^+ + e-……...8

$h^+ + OH^-$ ⟶ ·OH …….....9

$H^+ + H_2O$ ⟶ H^+ + ·OH…….....10

e- + O_2 ⟶ $\cdot O_2$ ……11

e- + $H^+ + O_2$ ⟶ H_2O_2 …….....12

e- + H_2O_2 ⟶ ·OH + OH- ……13

·OH/$\cdot O_2$ + MB ⟶ $CO_2 + H_2O$ …….. 14

5. CONCLUSION AND RECOMMENDATIONS

5.1 Conclusion

In this study, highly crystalline Cu_2O/graphene nanocomposites were synthesized via sol-gel method. XRD confirms the formation of the pure Cu_2O phase and analysis indicates that cuprous oxide nanoparticles on graphene have an average size of ~24.3nm with a cubic structure. The SEM images indicated the graphene sheets were decorated by spherical Cu_2O particles which were distributed randomly on the surface and edges of the graphene sheets. Optical band gap of Cu_2O/graphene nanocomposite is found to be 1.96 eV, with direct bandgap transition. Moreover, the photocatalytic efficiency of the synthesized Cu_2O nanoparticle towards MB dye is found to be improved when coupled with Graphene. Cu_2O/graphene nanocomposite and Cu_2O nanoparticles showed 94 % and 67% degradation of MB solution in 180 min., respectively, showing excellent photocatalytic performance of Cu_2O/graphene in comparison with bare Cu_2O degradation efficiency. The degradation follows second-order kinetics with a rate constant of 0.0085 and 0.053 $M^{-1}.min^{-1}$ for Cu_2O and Cu_2O/graphene nanocomposite, showing a better photodegradation rate of MB dye under Cu_2O/graphene nanocomposite. Therefore, Cu_2O/graphene nanocomposite was found to be promising in its photodegradation and reusability for MB removal.

5.2 Recommendation

The initial optimized parameters for synthesis and photodegradation of Cu_2O/graphene photocatalyst exhibit different efficiency under different conditions. This shows the promise of these materials in photocatalytic applications. The future work should focus on:

- Further synthesizing the Cu_2O/graphene nanocomposite using different methods such as hydrothermal and compare catalyst efficiency and differences under similar conditions.
- Further material characterization like TEM, EDX and Spectroscopy characterization techniques like Raman spectroscopy should be performed to fully understand its property which could not be performed due to equipment and financial limitations.
- Further investigation is needed to study the mechanism of removing methylene blue using this photocatalyst.

6. REFERENCES

[1] Beura, R.; Thangadurai, P. Structural, Optical and Photocatalytic Properties of Graphene-ZnO Nanocomposites for Varied Compositions. *J. Phys. Chem. Solids*. **2017**, *102*, 168–177.

[2] Amarah, J. O. M. Removal of Methylene Blue from Industrial Wastewater in Palestine Using Polysiloxane Surface Modified with Bipyrazolic Tripodal Receptor. PhD Thesis. 2015.

[3] Tichapondwa, S. M.; Newman, J. P.; Kubheka, O. Effect of TiO2 Phase on the Photocatalytic Degradation of Methylene Blue Dye. *Phys. Chem. Earth Parts ABC*. **2020**, *118*, 102900.

[4] Aragaw, B. A.; Dagnaw, A. Copper/Reduced Graphene Oxide Nanocomposite for High Performance Photocatalytic Methylene Blue Dye Degradation. *Ethiop. J. Sci. Technol.* **2019**, *12* (2), 125–137.

[5] Akerdi, A. G.; Bahrami, S. H. Application of Heterogeneous Nano-Semiconductors for Photocatalytic Advanced Oxidation of Organic Compounds: A Review. *J. Environ. Chem. Eng.* **2019**, *7* (5), 103283.

[6] Varjani, S. J. Microbial Degradation of Petroleum Hydrocarbons. *Bioresour. Technol.* **2017**, *223*, 277–286.

[7] Letort, S.; Bosco, M.; Cornelio, B.; Brégier, F.; Daulon, S.; Gouhier, G.; Estour, F. Structure–Efficiency Relationships of Cyclodextrin Scavengers in the Hydrolytic Degradation of Organophosphorus Compounds. *Beilstein J. Org. Chem.* **2017**, *13* (1), 417–427.

[8] Li, Q.; Xue, D.-X.; Zhang, Y.-F.; Zhang, Z.-H.; Gao, Z.; Bai, J. A Dual-Functional Indium–Organic Framework towards Organic Pollutant Decontamination via Physically Selective Adsorption and Chemical Photodegradation. *J. Mater. Chem. A.* **2017**, *5* (27), 14182–14189.

[9] Ashraf, M. A.; Liu, Z.; Peng, W.-X.; Jermsittiparsert, K.; Hosseinzadeh, G.; Hosseinzadeh, R. Combination of Sonochemical and Freeze-Drying Methods for Synthesis of Graphene/Ag-Doped TiO_2 Nanocomposite: A Strategy to Boost the Photocatalytic

Performance via Well Distribution of Nanoparticles between Graphene Sheets. *Ceram. Int.* **2020**, *46* (6), 7446–7452.

[10] Lin, C.; Gao, Y.; Zhang, J.; Xue, D.; Fang, H.; Tian, J.; Zhou, C.; Zhang, C.; Li, Y.; Li, H. GO/TiO_2 Composites as a Highly Active Photocatalyst for the Degradation of Methyl Orange. *J. Mater. Res.* **2020**, *35* (10), 1307–1315.

[11] Wang, T.; Dissanayake, P. D.; Sun, M.; Tao, Z.; Han, W.; An, N.; Gu, Q.; Xia, D.; Tian, B.; Ok, Y. S. Adsorption and Visible-Light Photocatalytic Degradation of Organic Pollutants by Functionalized Biochar: Role of Iodine Doping and Reactive Species. *Environ. Res.* **2021**, *197*, 111026.

[12] Bresolin, B.-M.; Hammouda, S. B.; Sillanpää, M. Methylammonium Iodo Bismuthate Perovskite (CH_3NH_3) $3Bi_2I_9$ as New Effective Visible Light-Responsive Photocatalyst for Degradation of Environment Pollutants. *J. Photochem. Photobiol. Chem.* **2019**, *376*, 116–126.

[13] Chong, M. N.; Jin, B.; Chow, C. W.; Saint, C. Recent Developments in Photocatalytic Water Treatment Technology: A Review. *Water Res.* **2010**, *44* (10), 2997–3027.

[14] Singh, P.; Shandilya, P.; Raizada, P.; Sudhaik, A.; Rahmani-Sani, A.; Hosseini-Bandegharaei, A. Review on Various Strategies for Enhancing Photocatalytic Activity of Graphene Based Nanocomposites for Water Purification. *Arab. J. Chem.* **2020**, *13* (1), 3498–3520.

[15] Liu, L.; Bai, H.; Liu, J.; Sun, D. D. Multifunctional Graphene Oxide-TiO_2-Ag Nanocomposites for High Performance Water Disinfection and Decontamination under Solar Irradiation. *J. Hazard. Mater.* **2013**, *261*, 214–223.

[16] Akbal, F. Photocatalytic Degradation of Organic Dyes in the Presence of Titanium Dioxide under UV and Solar Light: Effect of Operational Parameters. *Environ. Prog.* **2005**, *24* (3), 317–322.

[17] Rajamanickam, D.; Shanthi, M. Photocatalytic Degradation of an Organic Pollutant by Zinc Oxide–Solar Process. *Arab. J. Chem.* **2016**, *9*, S1858–S1868.

[18] Zhang, Z.; Hossain, M. F.; Takahashi, T. Self-Assembled Hematite (α-Fe_2O_3) Nanotube Arrays for Photoelectrocatalytic Degradation of Azo Dye under Simulated Solar Light Irradiation. *Appl. Catal. B Environ.* **2010**, *95* (3–4), 423–429.

[19] Carcel, R. A.; Andronic, L.; Duta, A. Photocatalytic Degradation of Methylorange Using TiO_2, WO_3 and Mixed Thin Films under Controlled PH and H_2O_2. *J. Nanosci. Nanotechnol.* **2011**, *11* (10), 9095–9101.

[20] Nezamzadeh-Ejhieh, A.; Karimi-Shamsabadi, M. Comparison of Photocatalytic Efficiency of Supported CuO onto Micro and Nano Particles of Zeolite X in Photodecolorization of Methylene Blue and Methyl Orange Aqueous Mixture. *Appl. Catal. Gen.*, **2014**, *477*, 83–92.

[21] Zhang, D.; Hu, B.; Guan, D.; Luo, Z. Essential Roles of Defects in Pure Graphene/Cu_2O Photocatalyst. *Catal. Commun.* **2016**, *76*, 7–12.

[22] Zheng, Y.; Wang, Z.; Peng, F.; Wang, A.; Cai, X.; Fu, L. Growth of Cu_2O Nanoparticle on Reduced Graphene Sheets with High Photocatalytic Activity for Degradation of Rhodamine B. *Fuller. Nanotub. Carbon Nanostructures*. **2016**, *24* (2), 149–153.

[23] Luévano-Hipólito, E.; Torres-Martínez, L. M.; Sánchez-Martínez, D.; Cruz, M. A. Cu2O Precipitation-Assisted with Ultrasound and Microwave Radiation for Photocatalytic Hydrogen Production. *Int. J. Hydrog. Energy*. **2017**, *42* (18), 12997–13010.

[24] Murphin Kumar, P. S.; Al-Muhtaseb, A. H.; Kumar, G.; Vinu, A.; Cha, W.; Villanueva Cab, J.; Pal, U.; Krishnan, S. K. Piper Longum Extract-Mediated Green Synthesis of Porous Cu_2O: Mo Microspheres and Their Superior Performance as Active Anode Material in Lithium-Ion Batteries. *ACS Sustain. Chem. Eng.* **2020**, *8* (38), 14557–14567.

[25] Gemeay, A.; El-Halwagy, M. Immobilization Impact of Photocatalysts onto Graphene Oxide. In *Graphene Oxide-Applications and Opportunities*; IntechOpen. 2018.

[26] Adam, R. E.; Chalangar, E.; Pirhashemi, M.; Pozina, G.; Liu, X.; Palisaitis, J.; Pettersson, H.; Willander, M.; Nur, O. Graphene-Based Plasmonic Nanocomposites for Highly Enhanced Solar-Driven Photocatalytic Activities. *RSC Adv.* **2019**, *9* (52), 30585–30598.

[27] Yan, J.; Fan, Y.; Lian, J.; Zhao, Y.; Xu, Y.; Gu, J.; Song, Y.; Xu, H.; Li, H. Kinetics and Mechanism of Enhanced Photocatalytic Activity Employing ZnS Nanospheres/Graphene-like C_3N4. *Mol. Catal.* **2017**, *438*, 103–112.

[28] Mei, W.; Lin, M.; Chen, C.; Yan, Y.; Lin, L. Low-Temperature Synthesis and Sunlight-Catalytic Performance of Flower-like Hierarchical Graphene Oxide/ZnO Macrosphere. *J. Nanoparticle Res.* **2018**, *20* (11), 1–12.

[29] Zhou, K.; Zhu, Y.; Yang, X.; Jiang, X.; Li, C. Preparation of Graphene–TiO_2 Composites with Enhanced Photocatalytic Activity. *New J. Chem.* **2011**, *35* (2), 353–359.

[30] Dasineh Khiavi, N.; Katal, R.; Kholghi Eshkalak, S.; Masudy-Panah, S.; Ramakrishna, S.; Jiangyong, H. Visible Light Driven Heterojunction Photocatalyst of CuO–Cu_2O Thin Films for Photocatalytic Degradation of Organic Pollutants. *Nanomaterials*. **2019**, *9* (7), 1011.

[31] Abdellah, M. H.; Nosier, S. A.; El-Shazly, A. H.; Mubarak, A. A. Photocatalytic Decolorization of Methylene Blue Using TiO_2/UV System Enhanced by Air Sparging. *Alex. Eng. J.* **2018**, *57* (4), 3727–3735.

[32] Low, S.; Shon, Y.-S. Molecular Interactions between Pre-Formed Metal Nanoparticles and Graphene Families. *Adv. Nano Res.* **2018**, *6* (4), 357–375.

[33] Martins, P. M.; Ferreira, C. G.; Silva, A. R.; Magalhães, B.; Alves, M. M.; Pereira, L.; Marques, P. A. A. P.; Melle-Franco, M.; Lanceros-Méndez, S. TiO_2/Graphene and TiO_2/Graphene Oxide Nanocomposites for Photocatalytic Applications: A Computer Modeling and Experimental Study. *Compos. Part B Eng.* **2018**, *145*, 39–46.

[34] Vasanthakumar, V.; Priyadharsan, A.; Anbarasan, P. M.; Muthumari, S.; Subramanian, S.; Raj, V. Enhancing Toxic Metal Ions and Dye Removal Properties of Nanostructured Terpolymer Formed by Diaminodiphenylmethane-Resorcinol-Formaldehyde. *ChemistrySelect*. **2017**, *2* (29), 9501–9510.

[35] Vinodgopal, K.; Wynkoop, D. E.; Kamat, P. V. Environmental Photochemistry on Semiconductor Surfaces: Photosensitized Degradation of a Textile Azo Dye, Acid Orange 7, on TiO_2 Particles Using Visible Light. *Environ. Sci. Technol.* **1996**, *30* (5), 1660–1666.

[36] Priyadharsan, A.; Vasanthakumar, V.; Shanavas, S.; Karthikeyan, S.; Anbarasan, P. M. Crumpled Sheet like Graphene Based WO_3-Fe_2O_3 Nanocomposites for Enhanced Charge Transfer and Solar Photocatalysts for Environmental Remediation. *Appl. Surf. Sci.* **2019**, *470*, 114–128.

[37] Gautam, S.; Agrawal, H.; Thakur, M.; Akbari, A.; Sharda, H.; Kaur, R.; Amini, M. Metal Oxides and Metal Organic Frameworks for the Photocatalytic Degradation: A Review. *J. Environ. Chem. Eng.* **2020**, *8* (3), 103726.

[38] Paracchino, A.; Laporte, V.; Sivula, K.; Grätzel, M.; Thimsen, E. Highly Active Oxide Photocathode for Photoelectrochemical Water Reduction. *Nat. Mater.* **2011**, *10* (6), 456–461.

[39] Wu, L.; Wan, G.; Hu, N.; He, Z.; Shi, S.; Suo, Y.; Wang, K.; Xu, X.; Tang, Y.; Wang, G. Synthesis of Porous $CoFe_2O_4$ and Its Application as a Peroxidase Mimetic for Colorimetric Detection of H_2O_2 and Organic Pollutant Degradation. *Nanomaterials*. **2018**, *8* (7), 451.

[40] Vlassiouk, I.; Polizos, G.; Cooper, R.; Ivanov, I.; Keum, J. K.; Paulauskas, F.; Datskos, P.; Smirnov, S. Strong and Electrically Conductive Graphene-Based Composite Fibers and Laminates. *ACS Appl. Mater. Interfaces*. **2015**, *7* (20), 10702–10709.

[41] Bolotin, K. I.; Sikes, K. J.; Jiang, Z.; Klima, M.; Fudenberg, G.; Hone, J. ea; Kim, P.; Stormer, H. L. Ultrahigh Electron Mobility in Suspended Graphene. *Solid State Commun.* **2008**, *146* (9–10), 351–355.

[42] Stoller, M. D.; Park, S.; Zhu, Y.; An, J.; Ruoff, R. S. Graphene-Based Ultracapacitors. *Nano Lett.*, **2008**, *8* (10), 3498–3502.

[43] Laurent, S.; Forge, D.; Port, M.; Roch, A.; Robic, C.; Vander Elst, L.; Muller, R. N. Magnetic Iron Oxide Nanoparticles: Synthesis, Stabilization, Vectorization, Physicochemical Characterizations, and Biological Applications. *Chem. Rev.* **2008**, *108* (6), 2064–2110.

[44] Shin, W.-K.; Cho, J.; Kannan, A. G.; Lee, Y.-S.; Kim, D.-W. Cross-Linked Composite Gel Polymer Electrolyte Using Mesoporous Methacrylate-Functionalized SiO_2 Nanoparticles for Lithium-Ion Polymer Batteries. *Sci. Rep.* **2016**, *6* (1), 1–10.

[45] Thanh, N. T.; Maclean, N.; Mahiddine, S. Mechanisms of Nucleation and Growth of Nanoparticles in Solution. *Chem. Rev.* **2014**, *114* (15), 7610–7630.

[46] Koczkur, K. M.; Mourdikoudis, S.; Polavarapu, L.; Skrabalak, S. E. Polyvinylpyrrolidone (PVP) in Nanoparticle Synthesis. *Dalton Trans.* **2015**, *44* (41), 17883–17905.

[47] Kumar, D. D. Nanoworld of Science and Technology. *The Chemist*. **2006**, *83* (1), 7–10.

[48] Pal, S. L.; Jana, U.; Manna, P. K.; Mohanta, G. P.; Manavalan, R. Nanoparticle: An Overview of Preparation and Characterization. *J. Appl. Pharm. Sci.* **2011**, *1* (6), 228–234.

[49] Hagens, W. I.; Oomen, A. G.; de Jong, W. H.; Cassee, F. R.; Sips, A. J. What Do We (Need to) Know about the Kinetic Properties of Nanoparticles in the Body? *Regul. Toxicol. Pharmacol.* **2007**, *49* (3), 217–229.

[50] Esencan Turkaslan, B.; Filiz Aydin, M. Optimizing Parameters of Graphene Derivatives Synthesis by Modified Improved Hummers. *Math. Methods Appl. Sci.* **2020**.

[51] Choi, W.; Lahiri, I.; Seelaboyina, R.; Kang, Y. S. Synthesis of Graphene and Its Applications: A Review. *Crit. Rev. Solid State Mater. Sci.* **2010**, *35* (1), 52–71.

[52] Zaaba, N. I.; Foo, K. L.; Hashim, U.; Tan, S. J.; Liu, W.-W.; Voon, C. H. Synthesis of Graphene Oxide Using Modified Hummers Method: Solvent Influence. *Procedia Eng.* **2017**, *184*, 469–477.

[53] Geim, A. K.; Novoselov, K. S. The Rise of Graphene. In *Nanoscience and technology: a collection of reviews from nature journals*; World Scientific. 2010; pp 11–19.

[54] Gaikwad, M. S.; Balomajumder, C. Capacitive Deionization for Desalination Using Nanostructured Electrodes. *Anal. Lett.* **2016**, *49* (11), 1641–1655.

[55] Banerjee, A. N. Graphene and Its Derivatives as Biomedical Materials: Future Prospects and Challenges. *Interface Focus*. **2018**, *8* (3), 20170056.

[56] Fu, L.; Liao, K.; Tang, B.; Jiang, L.; Huang, W. Applications of Graphene and Its Derivatives in the Upstream Oil and Gas Industry: A Systematic Review. *Nanomaterials*. **2020**, *10* (6), 1013.

[57] Tahriri, M.; Del Monico, M.; Moghanian, A.; Yaraki, M. T.; Torres, R.; Yadegari, A.; Tayebi, L. Graphene and Its Derivatives: Opportunities and Challenges in Dentistry. *Mater. Sci. Eng. C.* **2019**, *102*, 171–185.

[58] Singh, N.; Prakash, J.; Gupta, R. K. Design and Engineering of High-Performance Photocatalytic Systems Based on Metal Oxide–Graphene–Noble Metal Nanocomposites. *Mol. Syst. Des. Eng.* **2017**, *2* (4), 422–439.

[59] Upadhyay, R. K.; Soin, N.; Roy, S. S. Role of Graphene/Metal Oxide Composites as Photocatalysts, Adsorbents and Disinfectants in Water Treatment: A Review. *RSC Adv.* **2013**, *4* (8), 3823–3851.

[60] Liu, S.-H.; Lu, J.-S. Facet-Dependent Cuprous Oxide Nanocrystals Decorated with Graphene as Durable Photocatalysts under Visible Light. *Nanomaterials*. **2018**, *8* (6), 423.

[61] Paracchino, A.; Laporte, V.; Sivula, K.; Grätzel, M.; Thimsen, E. Highly Active Oxide Photocathode for Photoelectrochemical Water Reduction. *Nat. Mater.* **2011**, *10* (6), 456–461.

[62] Wu, Z. Nanocarbon-Based Photocatalysts: RGO/Metal Oxides Composite Membranes. **2017**.

[63] Ge, J.; Zhang, Y.; Park, S.-J. Recent Advances in Carbonaceous Photocatalysts with Enhanced Photocatalytic Performances: A Mini Review. *Materials*. **2019**, *12* (12), 1916.

[64] Sun, L.; Wang, G.; Hao, R.; Han, D.; Cao, S. Solvothermal Fabrication and Enhanced Visible Light Photocatalytic Activity of Cu2O-Reduced Graphene Oxide Composite Microspheres for Photodegradation of Rhodamine B. *Appl. Surf. Sci.* **2015**, *358*, 91–99.

[65] Li, B.; Liu, T.; Hu, L.; Wang, Y. A Facile One-Pot Synthesis of Cu_2O/RGO Nanocomposite for Removal of Organic Pollutant. *J. Phys. Chem. Solids*. **2013**, *74* (4), 635–640.

[66] Sophia, A. C.; Arfin, T.; Lima, E. C. Recent Developments in Adsorption of Dyes Using Graphene Based Nanomaterials. In *A New Generation Material Graphene: Applications in Water Technology*; Springer. 2019; pp 439–471.

[67] Dhand, V.; Rhee, K. Y.; Ju Kim, H.; Ho Jung, D. A Comprehensive Review of Graphene Nanocomposites: Research Status and Trends. *J. Nanomater.* **2013**, *2013*.

[68] Khan, M.; Tahir, M. N.; Adil, S. F.; Khan, H. U.; Siddiqui, M. R. H.; Al-warthan, A. A.; Tremel, W. Graphene Based Metal and Metal Oxide Nanocomposites: Synthesis, Properties and Their Applications. *J. Mater. Chem. A.* **2015**, *3* (37), 18753–18808.

[69] Kerour, A.; Boudjadar, S.; Bourzami, R.; Allouche, B. Eco-Friendly Synthesis of Cuprous Oxide (Cu_2O) Nanoparticles and Improvement of Their Solar Photocatalytic Activities. *J. Solid State Chem.* **2018**, *263*, 79–83.

[70] Mohd Shah, R.; Mohamad Yunus, R.; Masdar@Mastar, M. S.; Jefferey Minggu, L.; Wong, W. Y.; H. Kadhum, A. A. Synthesis of Graphene/CU_2O Thin Film Photoelectrode via Facile Hydrothermal Method for Photoelectrochemical Measurement. *Sains Malays.* **2019**, *48* (6), 1233–1238.

[71] Atkins, P.; Overton, T. *Shriver and Atkins' Inorganic Chemistry*; Oxford University Press, USA. 2010.

[72] Mourdikoudis, S.; Pallares, R. M.; Thanh, N. T. Characterization Techniques for Nanoparticles: Comparison and Complementarity upon Studying Nanoparticle Properties. *Nanoscale*. **2018**, *10* (27), 12871–12934.

[73] Raliya, R.; Tarafdar, J. C. Biosynthesis and Characterization of Nanoparticles. *Curr. TRENDS Adv. Sci. Res. Opin. Appl. Res. Opin. Appl. Microbiol. Biotechnol.* **2013**, 6.

[74] Srivastava, R. Synthesis and Characterization Techniques of Nanomaterials. *Int. J. Green Nanotechnol.* **2012**, *4* (1), 17–27.

[75] Mayence, A. Design and Characterization of Nanoparticles and Their Assemblies: Transmission Electron Microscopy Investigations from Atomic to Mesoscopic Length Scales. PhD Thesis, Department of Materials and Environmental Chemistry (MMK), Stockholm University. 2016.

[76] Rao, C. N. R.; Biswas, K. Characterization of Nanomaterials by Physical Methods. *Annu. Rev. Anal. Chem.* **2009**, *2*, 435–462.

[77] Heera, P.; Shanmugam, S. Nanoparticle Characterization and Application: An Overview. *Int J Curr Microbiol App Sci*. **2015**, *4* (8), 379–386.

[78] Dash, B. Competitive Adsorption of Dyes (Congo Red, Methylene Blue, Malachite Green) on Activated Carbon. PhD Thesis. 2010.

[79] Melhem, A. M. R. Synthesis and Characterization of Magnetic Nano Cellulose from Olive Waste (Jeft) for the Effective Removal of Methylene Blue from Water. PhD Thesis, An-Najah National University. 2017.

[80] Senthilkumaar, S.; Varadarajan, P. R.; Porkodi, K.; Subbhuraam, C. V. Adsorption of Methylene Blue onto Jute Fiber Carbon: Kinetics and Equilibrium Studies. *J. Colloid Interface Sci.* **2005**, *284* (1), 78–82.

[81] Linsebigler, A. L.; Lu, G.; Yates Jr, J. T. Photocatalysis on TiO_2 Surfaces: Principles, Mechanisms, and Selected Results. *Chem. Rev.* **1995**, *95* (3), 735–758.

[82] Han, L.; Wang, P.; Dong, S. Progress in Graphene-Based Photoactive Nanocomposites as a Promising Class of Photocatalyst. *Nanoscale*. **2012**, *4* (19), 5814–5825.

[83] Sinar Mashuri, S. I.; Ibrahim, M. L.; Kasim, M. F.; Mastuli, M. S.; Rashid, U.; Abdullah, A. H.; Islam, A.; Asikin Mijan, N.; Tan, Y. H.; Mansir, N. Photocatalysis for Organic Wastewater Treatment: From the Basis to Current Challenges for Society. *Catalysts*. **2020**, *10* (11), 1260.

[84] Hu, C.; Lu, T.; Chen, F.; Zhang, R. A Brief Review of Graphene–Metal Oxide Composites Synthesis and Applications in Photocatalysis. *J. Chin. Adv. Mater. Soc.* **2013**, *1* (1), 21–39.

[85] Kaur, K.; Badru, R.; Singh, P. P.; Kaushal, S. Photodegradation of Organic Pollutants Using Heterojunctions: A Review. *J. Environ. Chem. Eng.* **2020**, *8* (2), 103666.

[86] Viswanathan, B. Photocatalytic Degradation of Dyes: An Overview. *Curr. Catal.* **2018**, *7* (2), 99–121.

[87] Qadri, M. Z.; Chandran, R. R.; Ravindra, S.; Velmurugan, V. Synthesis and Testing of Graphene/Cuprous Oxide Composite Based Nano Fluids for Engine-Coolants. *Mater. Today Proc.* **2015**, *2* (9, Part A), 4640–4645.

[88] Mehariw, B. SYNTHESIS AND CHARACTERIZATION OF COPPER OXIDE/REDUCED GRAPHENE OXIDE NANO COMPOSITE AND ITS PHOTOCATALYTIC DEGRADATION ACTIVITIES OF METHYLENE BLUE DYE. PhD Thesis. 2021.

[89] Yu, C.; Shu, Y.; Zhou, X.; Ren, Y.; Liu, Z. Multi-Branched Cu_2O Nanowires for Photocatalytic Degradation of Methyl Orange. *Mater. Res. Express*. **2018**, *5* (3), 035046.

[90] Eda, G.; Fanchini, G.; Chhowalla, M. Large-Area Ultrathin Films of Reduced Graphene Oxide as a Transparent and Flexible Electronic Material. *Nat. Nanotechnol.* **2008**, *3* (5), 270–274.

[91] Isai, K. A.; Shrivastava, V. S. Photocatalytic Degradation of Methylene Blue Using ZnO and 2% Fe–ZnO Semiconductor Nanomaterials Synthesized by Sol–Gel Method: A Comparative Study. *SN Appl. Sci.* **2019**, *1* (10), 1–11.

[92] Echabbi, F.; Hamlich, M.; Harkati, S.; Jouali, A.; Tahiri, S.; Lazar, S.; Lakhmiri, R.; Safi, M. Photocatalytic Degradation of Methylene Blue by the Use of Titanium-Doped Calcined Mussel Shells CMS/TiO_2. *J. Environ. Chem. Eng.* **2019**, *7* (5), 103293.

[93] Khairnar, S. D.; Patil, M. R.; Shrivastava, V. S. Hydrothermally Synthesized Nanocrystalline Nb2O5 and Its Visible-Light Photocatalytic Activity for the Degradation of Congo Red and Methylene Blue. *Iran. J. Catal.* **2018**, *8* (2), 143–150.

[94] Handayani, M.; Ganta, M.; Susilo, D. N. A.; Yahya, M. S.; Sunnardianto, G. K.; Darsono, N.; Sulistiyono, E.; Setiawan, I.; Lestari, F. P.; Erryani, A. Synthesis of Graphene Oxide from Used Electrode Graphite with Controlled Oxidation Process. In *IOP Conference Series: Materials Science and Engineering*; IOP Publishing. 2019; Vol. 541, p 012032.

[95] Shahriary, L.; Athawale, A. A. Graphene Oxide Synthesized by Using Modified Hummers Approach. *Int J Renew Energy Env. Eng*. **2014**, *2* (01), 58–63.

[96] Huang, N. M.; Lim, H. N.; Chia, C. H.; Yarmo, M. A.; Muhamad, M. R. Simple Room-Temperature Preparation of High-Yield Large-Area Graphene Oxide. *Int. J. Nanomedicine*. **2011**, *6*, 3443.

[97] Stankovich, S.; Dikin, D. A.; Piner, R. D.; Kohlhaas, K. A.; Kleinhammes, A.; Jia, Y.; Wu, Y.; Nguyen, S. T.; Ruoff, R. S. Synthesis of Graphene-Based Nanosheets via Chemical Reduction of Exfoliated Graphite Oxide. *carbon*. **2007**, *45* (7), 1558–1565.

[98] Emiru, T. F.; Ayele, D. W. Controlled Synthesis, Characterization and Reduction of Graphene Oxide: A Convenient Method for Large Scale Production. *Egypt. J. Basic Appl. Sci.* **2017**, *4* (1), 74–79.

[99] Eigler, S.; Hirsch, A. Chemistry with Graphene and Graphene Oxide—Challenges for Synthetic Chemists. *Angew. Chem. Int. Ed.* **2014**, *53* (30), 7720–7738.

[100] Dreyer, D. R.; Park, S.; Bielawski, C. W.; Ruoff, R. S. The Chemistry of Graphene Oxide. *Chem. Soc. Rev.* **2010**, *39* (1), 228–240.

[101] Li, B.; Liu, T.; Hu, L.; Wang, Y. A Facile One-Pot Synthesis of Cu_2O/RGO Nanocomposite for Removal of Organic Pollutant. *J. Phys. Chem. Solids*. **2013**, *74* (4), 635–640.

[102] Roy, I.; Bhattacharyya, A.; Sarkar, G.; Saha, N. R.; Rana, D.; Ghosh, P. P.; Palit, M.; Das, A. R.; Chattopadhyay, D. In Situ Synthesis of a Reduced Graphene Oxide/Cuprous Oxide Nanocomposite: A Reusable Catalyst. *RSC Adv.* **2014**, *4* (94), 52044–52052.

[103] Bolotin, K. I.; Sikes, K. J.; Jiang, Z.; Klima, M.; Fudenberg, G.; Hone, J.; Kim, P.; Stormer, H. L. Ultrahigh Electron Mobility in Suspended Graphene. *Solid State Commun.* **2008**, *146* (9–10), 351–355.

[104] Patra, J. K.; Baek, K.-H. Green Nanobiotechnology: Factors Affecting Synthesis and Characterization Techniques. *J. Nanomater.* **2014**, *2014*.

[105] Bala, N.; Saha, S.; Chakraborty, M.; Maiti, M.; Das, S.; Basu, R.; Nandy, P. Green Synthesis of Zinc Oxide Nanoparticles Using Hibiscus Subdariffa Leaf Extract: Effect of Temperature on Synthesis, Anti-Bacterial Activity and Anti-Diabetic Activity. *RSC Adv.* **2015**, *5* (7), 4993–5003.

[106] Dada, A. O.; Adekola, F. A.; Adeyemi, O. S.; Bello, O. M.; Oluwaseun, A. C.; Awakan, O. J.; Grace, F.-A. A. Exploring the Effect of Operational Factors and Characterization Imperative to the Synthesis of Silver Nanoparticles. In *Silver Nanoparticles - Fabrication, Characterization and Applications*; Maaz, K., Ed.; InTech. 2018.

[107] Baer, D. R. Surface Characterization of Nanoparticles: Critical Needs and Significant Challenges. *J Surf. Anal*. **2011**, *17*, 163–169.

[108] An, X.; Li, K.; Tang, J. Cu_2O/Reduced Graphene Oxide Composites for the Photocatalytic Conversion of CO_2. *ChemSusChem*. **2014**, *7* (4), 1086–1093.

[109] Atarod, M.; Nasrollahzadeh, M.; Sajadi, S. M. Green Synthesis of a Cu/Reduced Graphene Oxide/Fe_3O_4 Nanocomposite Using Euphorbia Wallichii Leaf Extract and Its

Application as a Recyclable and Heterogeneous Catalyst for the Reduction of 4-Nitrophenol and Rhodamine B. *RSC Adv.* **2015**, *5* (111), 91532–91543.

[110] Thangavel, S.; Elayaperumal, M.; Venugopal, G. Synthesis and Properties of Tungsten Oxide and Reduced Graphene Oxide Nanocomposites. *Mater. Express*. **2012**, *2* (4), 327–334.

[111] Mei, Q.; Zhang, K.; Guan, G.; Liu, B.; Wang, S.; Zhang, Z. Highly Efficient Photoluminescent Graphene Oxide with Tunable Surface Properties. *Chem. Commun.* **2010**, *46* (39), 7319–7321.

[112] Huang, W.-C.; Lyu, L.-M.; Yang, Y.-C.; Huang, M. H. Synthesis of Cu2O Nanocrystals from Cubic to Rhombic Dodecahedral Structures and Their Comparative Photocatalytic Activity. *J. Am. Chem. Soc.* **2012**, *134* (2), 1261–1267.

[113] Tran Thi, V. H.; Pham, T. N.; Pham, T. T.; Le, M. C. Synergistic Adsorption and Photocatalytic Activity under Visible Irradiation Using Ag-ZnO/GO Nanoparticles Derived at Low Temperature. *J. Chem.* **2019**, *2019*.

[114] Nine, M. J.; Munkhbayar, B.; Rahman, M. S.; Chung, H.; Jeong, H. Highly Productive Synthesis Process of Well Dispersed Cu_2O and Cu/Cu_2O Nanoparticles and Its Thermal Characterization. *Mater. Chem. Phys.* **2013**, *141* (2–3), 636–642.

[115] Hassan, S. M.; Ahmed, A. I.; Mannaa, M. A. Structural, Photocatalytic, Biological and Catalytic Properties of SnO_2/TiO_2 Nanoparticles. *Ceram. Int.* **2018**, *44* (6), 6201–6211.

[116] Rout, S. Synthesis and Characterization of CuO/Graphene Oxide Composite. PhD Thesis. 2013.

[117] Alibeyli, R.; Ata, A.; Topaç, E. Reduced Graphene Oxide Synthesis via Improved Hummers' Method. ISITES. 2014.

[118] Bhargava, R.; Khan, S. Enhanced Optical Properties of Cu2O Anchored on Reduced Graphene Oxide (RGO) Sheets. *J. Phys. Condens. Matter*. **2018**, *30* (33), 335703.

[119] Hidayah, N. M. S.; Liu, W.-W.; Lai, C.-W.; Noriman, N. Z.; Khe, C.-S.; Hashim, U.; Lee, H. C. Comparison on Graphite, Graphene Oxide and Reduced Graphene Oxide: Synthesis and Characterization. In *AIP Conference Proceedings*; AIP Publishing LLC. 2017; Vol. 1892, p 150002.

[120] Mishra, A. K.; Ramaprabhu, S. Carbon Dioxide Adsorption in Graphene Sheets. *AIP Adv.* **2011**, *1* (3), 032152.

[121] Akpan, U. G.; Hameed, B. H. Parameters Affecting the Photocatalytic Degradation of Dyes Using TiO_2-Based Photocatalysts: A Review. *J. Hazard. Mater.* **2009**, *170* (2–3), 520–529.

[122] Bouna, L.; Rhouta, B.; Maury, F. Physicochemical Study of Photocatalytic Activity of TiO_2 Supported Palygorskite Clay Mineral. *Int. J. Photoenergy*. **2013**, *2013*.

[123] Kaur, S.; Singh, V. Visible Light Induced Sonophotocatalytic Degradation of Reactive Red Dye 198 Using Dye Sensitized TiO_2. *Ultrason. Sonochem.* **2007**, *14* (5), 531–537.

[124] Cao, J.; Luo, B.; Lin, H.; Chen, S. Photocatalytic Activity of Novel AgBr/WO_3 Composite Photocatalyst under Visible Light Irradiation for Methyl Orange Degradation. *J. Hazard. Mater.* **2011**, *190* (1–3), 700–706.

[125] Kurniawan, T. A.; Mengting, Z.; Fu, D.; Yeap, S. K.; Othman, M. H. D.; Avtar, R.; Ouyang, T. Functionalizing TiO_2 with Graphene Oxide for Enhancing Photocatalytic Degradation of Methylene Blue (MB) in Contaminated Wastewater. *J. Environ. Manage.* **2020**, *270*, 110871.

[126] Alkaykh, S.; Mbarek, A.; Ali-Shattle, E. E. Photocatalytic Degradation of Methylene Blue Dye in Aqueous Solution by MnTiO3 Nanoparticles under Sunlight Irradiation. *Heliyon*. **2020**, *6* (4), 663.

[127] Dariani, R. S.; Esmaeili, A.; Mortezaali, A.; Dehghanpour, S. Photocatalytic Reaction and Degradation of Methylene Blue on TiO_2 Nano-Sized Particles. *Optik.* **2016**, *127* (18), 7143–7154.

[128] Akbari, A.; Sabouri, Z.; Hosseini, H. A.; Hashemzadeh, A.; Khatami, M.; Darroudi, M. Effect of Nickel Oxide Nanoparticles as a Photocatalyst in Dyes Degradation and Evaluation of Effective Parameters in Their Removal from Aqueous Environments. *Inorg. Chem. Commun.* **2020**, *115*, 107867.

[129] Yuan, C.; Hung, C.-H.; Li, H.-W.; Chang, W.-H. Photodegradation of Ibuprofen by TiO_2 Co-Doping with Urea and Functionalized CNT Irradiated with Visible Light–Effect of Doping Content and PH. *Chemosphere*. **2016**, *155*, 471–478.

[130] Zheng, Y.; Wang, Z.; Peng, F.; Wang, A.; Cai, X.; Fu, L. Growth of Cu_2O Nanoparticle on Reduced Graphene Sheets with High Photocatalytic Activity for Degradation of Rhodamine B. *Fuller. Nanotub. Carbon Nanostructures*. **2016**, *24* (2), 149–153.

[131] Zeng, W.; Gao, M.; Liu, K.; Li, C.; Cao, N.; Zhao, X.; Feng, J.; Ren, Y.; Wei, T. Boosting Charge Separation and Surface Defects for Superb Photocatalytic Activity of Magnesium Oxide/Graphene Nanosheets. *Appl. Surf. Sci.* **2021**, *535*, 147658.

[132] Wang, C. L. Fractional Kinetics of Photocatalytic Degradation. *J. Adv. Dielectr*. **2018**, *08* (05), 1850034.

[133] El-Yazeed, W. A.; El-Hakam, S. A.; Salah, A. A.; Ibrahim, A. A. Fabrication and Characterization of Reduced Graphene-$BiVO_4$ Nanocomposites for Enhancing Visible Light Photocatalytic and Antibacterial Activity. *J. Photochem. Photobiol. Chem.* **2021**, *417*, 113362.

[134] Siddiqa, A.; Masih, D.; Anjum, D.; Siddiq, M. Cobalt and Sulfur Co-Doped Nano-Size TiO2 for Photodegradation of Various Dyes and Phenol. *J. Environ. Sci.* **2015**, *37*, 100–109.

[135] Kumar, S.; Ojha, A. K. In-Situ Synthesis of Reduced Graphene Oxide Decorated with Highly Dispersed Ferromagnetic CdS Nanoparticles for Enhanced Photocatalytic Activity under UV Irradiation. *Mater. Chem. Phys.* **2016**, *171*, 126–136.

7. APPEDIX

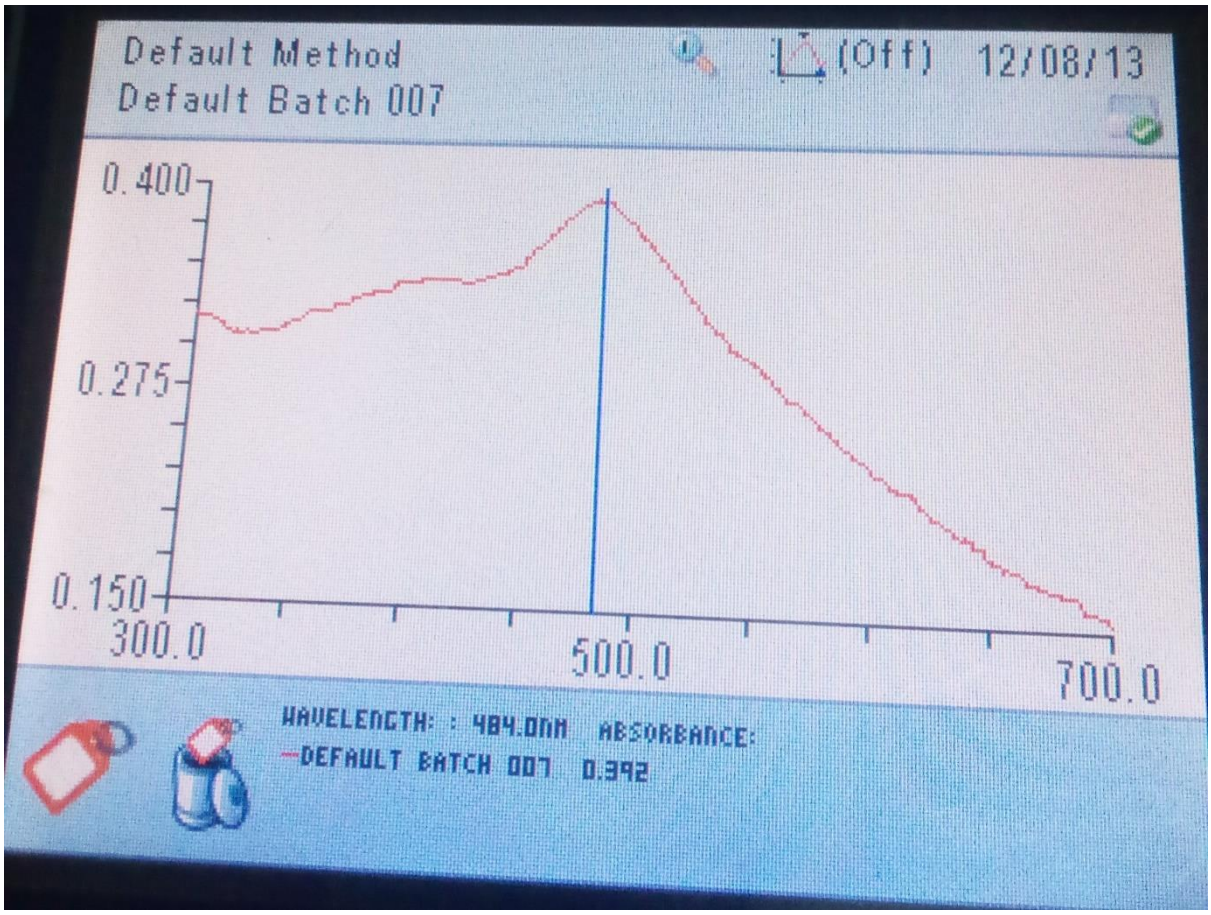
Default Method
Default Batch 007
(Off)
12/08/13
0.400
0.275
0.150
300.0
500.0
700.0
WAVELENGTH: : 484.0NM ABSORBANCE:
-DEFAULT BATCH 007 0.392

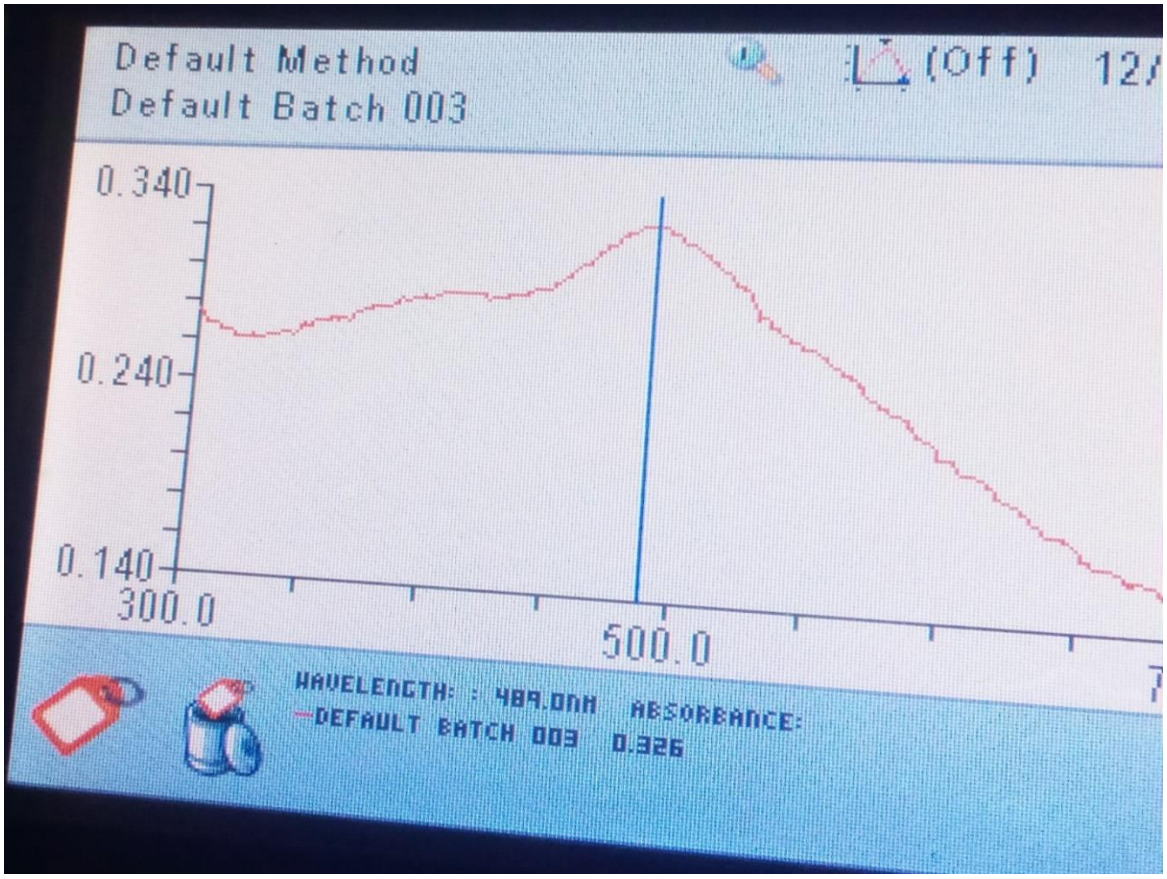
Default Method
Default Batch 003
(Off)
0.340
0.240
0.140
300.0
500.0
WAVELENGTH: : 489.0NM ABSORBANCE:
—DEFAULT BATCH 003 0.326

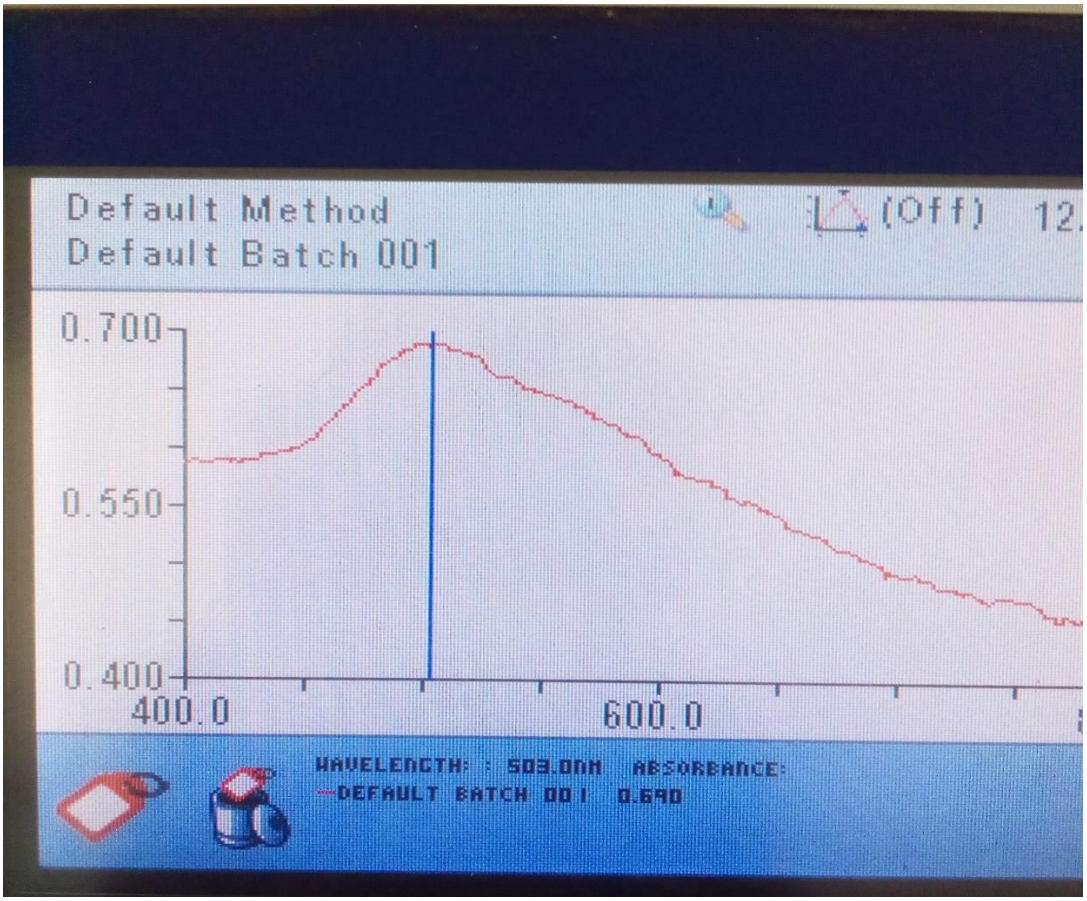
Default Method
Default Batch 001
(Off)
0.700
0.550
0.400
400.0
600.0
WAVELENGTH: : 503.0NM ABSORBANCE:
—DEFAULT BATCH 001 0.690

Appendix 1. Effect of GO content (a) 0.01 (b) 0.05 (c) 0.08

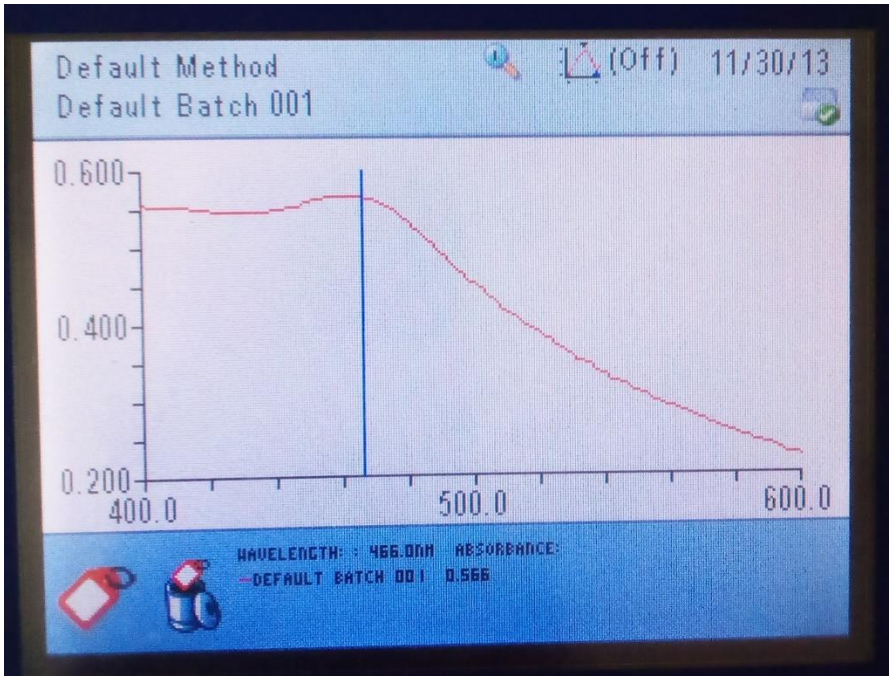

(a)

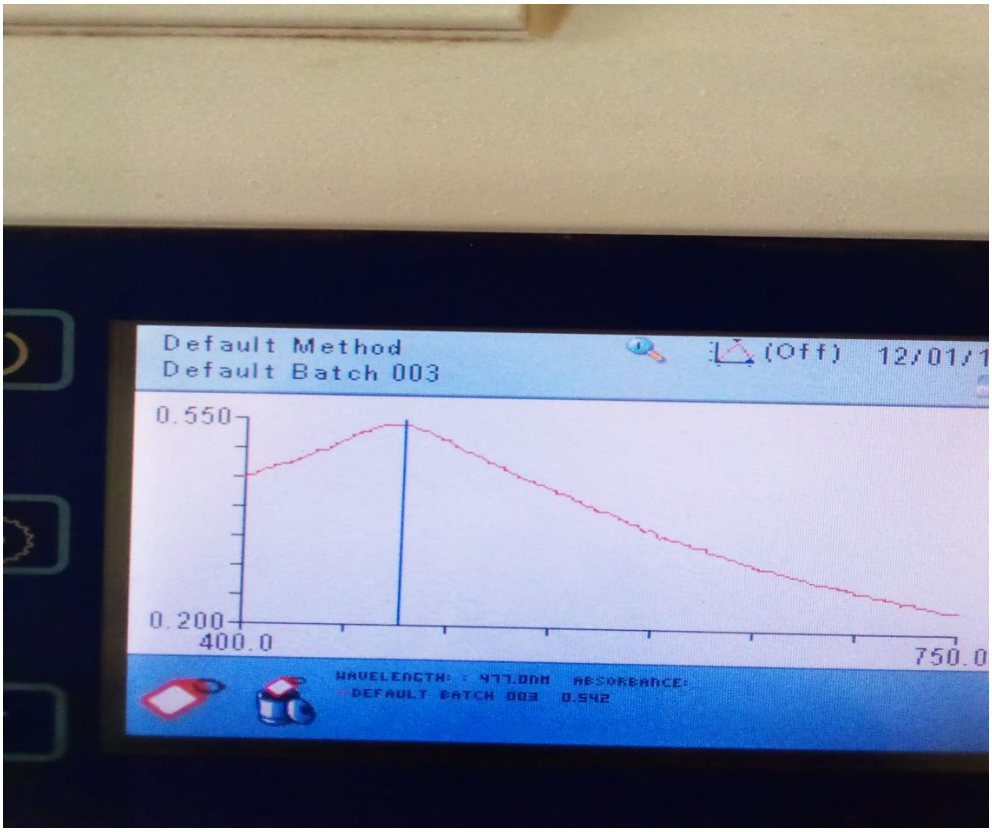

(b)

(c)

Appendix 2. Effect of temperature (a) at 60 (b) 80 and (c) 70 ^{0}c

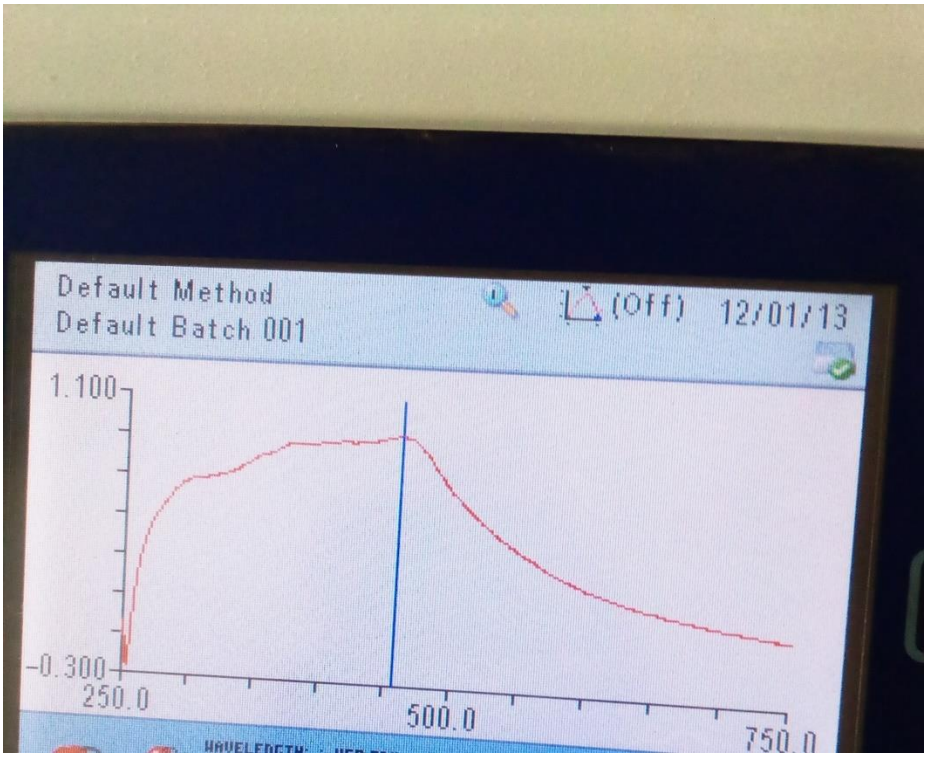
Default Method
Default Batch 001
(Off)
12/01/13
1.100
-0.300
250.0
500.0
750.0

(a)

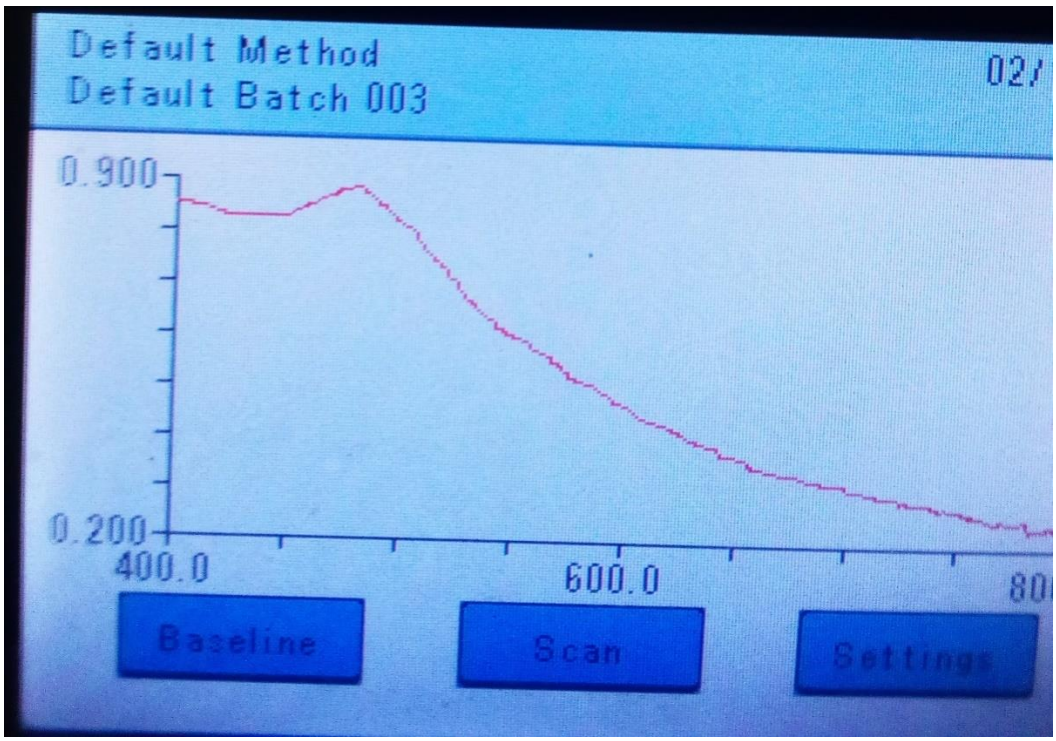
Default Method
Default Batch 003
02/
0.900
0.200
400.0
600.0
Baseline
Scan
Settings

(b)

(c)

Appendix 3. Effect of reaction time for (a) 1 h (b) 2 h and (c) 3h

parameters	Amount	K(min^{-1})	R^2
Catalyst Dosage	0.03 g	0.0052	0.9539
	0.05 g	0.0083	0.7329
	0.07 g	0.0131	0.5851
	0.09 g	0.0204	0.8521
PH	6	0.0062	0.9717
	8	0.0081	0.9734
	9	0.0101	0.906
	10	0.0171	0.989
	11	0.0115	0.806
Cu_2O/graphene	0.07 g	0.0339	0.903
Cu_2O	0.07 g	0.00456	0.925

Appendix 4. First-order rate constants and regression coefficients were obtained at different initial Cu_2O/graphene catalyst concentrations, and pH.

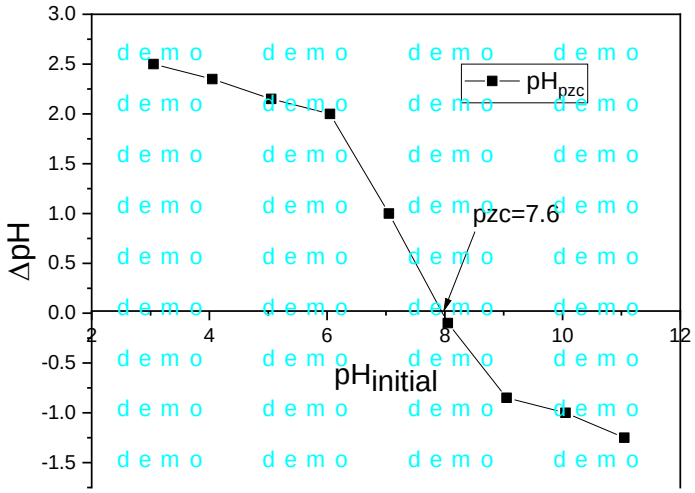

Appendix 5. Point of zero charge at ctalayst dosage 0.7 g/L, and 0.1 M of NaCl